

Review

Titanium Dioxide: From Engineering to Applications

Xiaolan Kang [†], Sihang Liu [†], Zideng Dai, Yunping He, Xuezhi Song and Zhenquan Tan ^{*ID}

School of Petroleum and Chemical Engineering, Dalian University of Technology, No. 2 Dagong Road, New District of Liaodong Bay, Panjin, Liaoning 124221, China; kxl@mail.dlut.edu.cn (X.K.); wdlld@mail.dlut.edu.cn (S.L.); xiaodai@mail.dlut.edu.cn (Z.D.); yphe_04@mail.dlut.edu.cn (Y.H.); songxz@dlut.edu.cn (X.S.)

* Correspondence: tanzq@dlut.edu.cn; Tel.: +86-427-263-1808

[†] These authors contributed equally to this work.

Received: 17 January 2019; Accepted: 10 February 2019; Published: 19 February 2019



Abstract: Titanium dioxide (TiO₂) nanomaterials have garnered extensive scientific interest since 1972 and have been widely used in many areas, such as sustainable energy generation and the removal of environmental pollutants. Although TiO₂ possesses the desired performance in utilizing ultraviolet light, its overall solar activity is still very limited because of a wide bandgap (3.0–3.2 eV) that cannot make use of visible light or light of longer wavelength. This phenomenon is a deficiency for TiO₂ with respect to its potential application in visible light photocatalysis and photoelectrochemical devices, as well as photovoltaics and sensors. The high overpotential, sluggish migration, and rapid recombination of photogenerated electron/hole pairs are crucial factors that restrict further application of TiO₂. Recently, a broad range of research efforts has been devoted to enhancing the optical and electrical properties of TiO₂, resulting in improved photocatalytic activity. This review mainly outlines state-of-the-art modification strategies in optimizing the photocatalytic performance of TiO₂, including the introduction of intrinsic defects and foreign species into the TiO₂ lattice, morphology and crystal facet control, and the development of unique mesocrystal structures. The band structures, electronic properties, and chemical features of the modified TiO₂ nanomaterials are clarified in detail along with details regarding their photocatalytic performance and various applications.

Keywords: TiO₂; energy band engineering; morphology modification; mesocrystals; applications

1. Introduction

Over the past several decades, the increasing severe energy shortages and environmental pollution have caused great concern worldwide. To achieve sustainable development of society, there is an urgent need to explore environmentally friendly technologies applicable to pollutant recovery and clean energy supplies. In the long-term, solar energy is an inexhaustible source of renewable energy; therefore, developing technologies and materials to enhance solar energy utilization is central to both energy security and environmental stewardship. In 1972, Fujishima and Honda first published a study for producing hydrogen on titanium dioxide (TiO₂) photoelectrodes under ultraviolet light illumination, which garnered worldwide attention [1,2]. From then on, semiconductor photocatalysis has been considered one of the most promising pathways to address both hydrogen production and pollution abatement. Photocatalysis can be widely used anywhere in the world, providing natural solar light or artificial indoor illumination is available [3].

Semiconductor materials are often used as photocatalysts [4]. According to band energy theory, the discontinuous band structure of semiconductors is composed of low energy valence bands filled with electrons, high-energy conduction bands, and band gaps. When the energy of the incident photons equals or exceeds the bandgap, the photoexcitation of electron–hole pairs and the consequential

photocatalytic redox reaction take place [5]. The photocatalytic process mainly involves the steps of generation, separation, recombination, and surface capture of photogenerated electrons and hole pairs. Photochemical reactions occur on the surface of a solid catalyst, which includes two half-reaction oxidation reactions of photogenerated holes and reduction reactions of photogenerated electrons [6]. The specific process that occurs in semiconductors is described in Figure 1. During this process, a large proportion of charge carriers (e^-/h^+ pairs) recombine quickly at the surface and interior of the bulk material, leading to the dissipation of absorbed energy in the form of light (photon generation) or heat (lattice vibration). Therefore, these charge carriers cannot participate in the subsequent photocatalytic reactions, which is detrimental to the whole process [7].

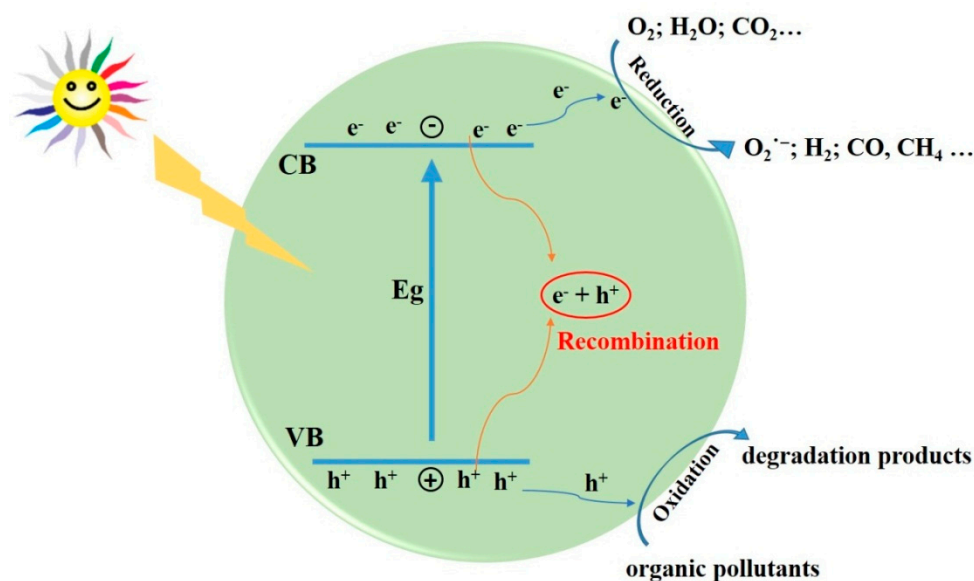


Figure 1. Photocatalytic process in semiconductor.

The electrons and holes that successfully migrate to the surface of the semiconductor without recombining can be involved in the reduction and oxidation reactions, respectively, which are the bases for photodegradation of organic pollutants and photocatalytic water splitting to produce H_2 [8]. As excellent oxidizers, the photogenerated holes can mineralize organic pollutants directly. In addition, the holes can also form hydroxyl radicals ($\bullet OH$) with strong oxidizing properties. Photoexcited electrons, on the other hand, can produce superoxide radicals ($O_2\bullet^-$) and $\bullet OH$. These free radicals and e^-/h^+ pairs are highly reactive and can induce a series of redox reactions. In addition, with respect to water splitting, photogenerated electrons can be captured by H^+ in water to generate hydrogen, while holes will oxidize H_2O to form O_2 [9–11].

In general, to increase the activity of photocatalysts and utilize visible light more effectively, several requirements need to be satisfied. First, the light absorption process determines the amount of excited charges, which means that more charge carriers are likely to be accumulated on the surface if more light can be absorbed by the photocatalyst. Additionally, considering that ultraviolet (UV) light occupies less than 4% of sunlight's emission spectrum, while visible light accounts for approximately 40%, a smaller bandgap is necessary for a semiconductor to absorb solar energy across a broad range of spectra. Therefore, improving the optical absorption properties has become a common purpose for photocatalyst design to enhance their overall activity [12]. In addition, the position of conduction bands (CBs) and valence bands (VBs) is critical, which are responsible for the production of active species, such as $\bullet OH$, $HO_2\bullet$, H_2O_2 , and $O_2\bullet^-$. Furthermore, the photogenerated electrons and holes should be transported and separated efficiently in the photocatalyst because the fast recombination of charge carriers will otherwise result in low reactivity. Finally, the as-prepared photocatalytic materials and their modification processes should be environmentally friendly and economical [13].

Since 1972, TiO₂ has been intensively investigated due to its thermal and chemical stability, superhydrophilicity, low toxicity, and natural geologic abundance. Compared with other semiconductor materials, TiO₂ is of ubiquitous interest across many research fields and for many applications [14], such as photodegradation of pollutants and hazardous materials, photolysis (splitting) of water to yield H₂, artificial photosynthesis, etc. Nevertheless, the poor visible light absorption and fast electron–hole recombination, as well as the sluggish transfer kinetics of the charge carriers to the surrounding media, considerably limit the photocatalytic activities of TiO₂. Hence, during the past few decades, much effort has been devoted to overcoming these problems by, for example, reducing e[−]/h⁺ pair recombination and improving the optical absorption properties by energy band regulation, morphology control, and the construction of heterogeneous junctions [15].

In this review, we mainly focus on the regulation of the electronic structure and modification of the micromorphology of TiO₂ nanomaterials to achieve property enhancements that could be applicable to a variety of potential applications.

2. Energy Band Engineering of TiO₂

The absorption of incident light and redox potential of TiO₂ mainly depend on its energy band configuration [16]. To utilize solar energy more effectively, it is necessary to explore and develop longwave-light-sensitive TiO₂ photocatalysts with excellent performance on the basis of energy band engineering [17]. A better understanding of the electronic structure of TiO₂ is important for band gap modification. The molecular orbital bonding energy diagram in Figure 2 clearly shows the fundamental features of anatase TiO₂ [18]. The chemical bonding of anatase TiO₂ can be deconstructed into Ti, e.g., Ti *t*_{2g} (*d*_{yz}, *d*_{xz}, and *d*_{xy}), O *p*_σ (in the Ti₃O cluster plane), and O *p*_π (out of the Ti₃O cluster plane). The upper valence bands include three main regions: the σ bonding, which is located at the bottom, is the most stable bond type, and arises from the hybridization of Ti, e.g., O *p*_σ; the hybridization of the O *p*_π and Ti *d*_{yz} (or *d*_{xz}) orbitals constitutes the middle energy region of π bonding; and the higher energy region in the top of the valence bands, which is dominated by the O *p*_π orbitals. The conduction band is composed of Ti 3d and 4s, and the bottom of the conduction bands is composed of the isolated Ti *d*_{xy} orbitals [19,20]. For the purpose of narrowing the bandgap of TiO₂, three basic approaches of adjusting the VBs or CBs or the continuous modification of the VBs and CBs of the anatase are shown in Figure 3.

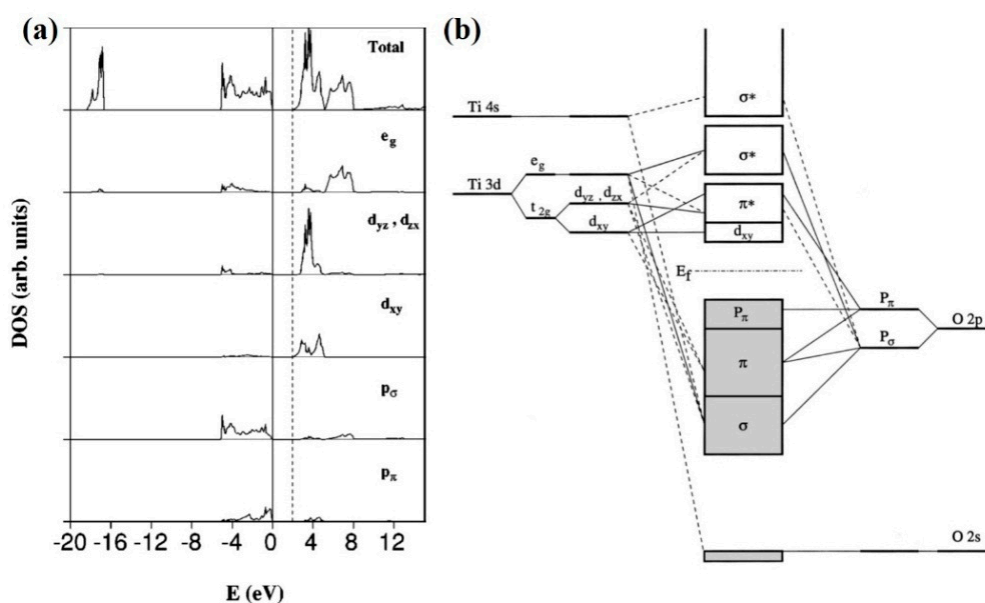


Figure 2. (a) Total and projected densities of states (DOS) of the anatase TiO₂ structure and (b) molecular orbital bonding structure for anatase TiO₂ [18]. Copyright 2004 The American Physical Society.

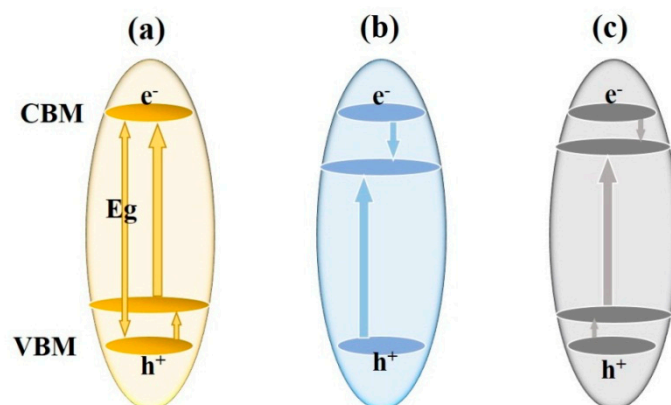


Figure 3. Three schemes of the band gap modifications of TiO_2 match the solar spectrum: (a) a higher shift in valence band maximum (VBM); (b) a lower shift in conduction band minimum (CBM); and (c) continuous modification of both VBM and CBM.

2.1. Doping of TiO_2

To extend the visible light response of TiO_2 and improve its photocatalytic activities, various modification strategies, such as dye sensitization, impurity or intrinsic doping or semiconductor coupling, have been developed [21–23]. Among them, introducing impurity ions into the TiO_2 crystal lattice to substitute the host anions and/or cations has earned much attention in the past decade.

By means of physical or chemical methods, researchers have been able to introduce a variety of ions into the TiO_2 matrix, where they change the band structure of TiO_2 by inducing impurity states within the bandgap [2], as shown in Figure 4. In general, ion doping contributes to the improved activities of TiO_2 in three ways: (1) by narrowing the bandgap and promoting the adsorption of the main region of the solar spectrum, such as doping with N, S, C, B, etc. [24,25]; (2) by improving the conductivity of TiO_2 and the mobility of charge carriers, the increased charge traps can reduce bulk recombination and separate photogenerated electrons and holes more efficiently (e.g., Zn, Fe, and Y) [26]; and (3) by altering the conduction band position of TiO_2 with certain metal ion dopants, such as Zr^{4+} , Nb^{5+} , and W^{6+} , which further affects the carrier transfer properties [27].

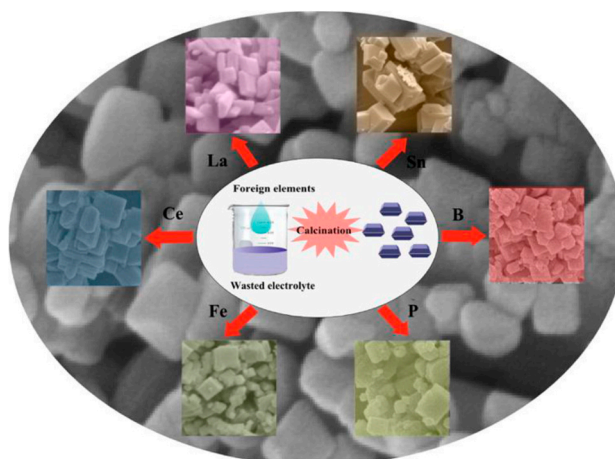


Figure 4. TiO_2 nanoparticles with different doping elements [2]. Copyright 2014 American Chemical Society.

TiO_2 doping can be doped with a variety of metal ions, including transition metal and rare earth metal ions. For transition metal dopants, such as Fe, Mn, V, Cu, and Cr, both delocalized and localized impurity states will be created within the band gap of TiO_2 along the crystal field splitting of metal 3d orbitals [28–30]. Mizushima et al. determined impurity levels of 1.9 to 3.0 eV below CBM by

doping V, Cr, Mn, and Fe based on a large number of experimental results, and they suggested that cation vacancies may lead to these impurity states [31]. An early work by Borgarello et al. in 1982 reported that Cr^{3+} -doped TiO_2 nanoparticles (investigated for properties of photocatalytic hydrogen evolution) exhibit excellent absorption of visible light in the range of 400 to 550 nm. They believed that the 3d electrons of Cr^{3+} were excited into the conduction band of TiO_2 , thus inducing a visible light response [32]. Doping TiO_2 with certain earth rare metal ions represents another promising method to prolong the recombination time of charge carriers and improve their separation efficiency. The 4f electrons in most rare earth elements can give rise to the formation of a multielectron configuration, which acts as a shallow trap for photogenerated electrons and holes [33]. Furthermore, the use of rare earth metal ion dopants in TiO_2 tends to facilitate the utilization of solar light from ultraviolet to infrared light regions. Li et al. prepared a series of Ce-doped TiO_2 nanoparticles by the sol–gel method. The characterization results showed that Ce ions entered the TiO_2 matrix at Ti sites, leading to the formation of impurity states, as shown in Figure 5. In addition, enhanced separation of the photogenerated charge carriers was also realized due to the coexistence of Ce^{3+} and Ce^{4+} dopant ions [34].

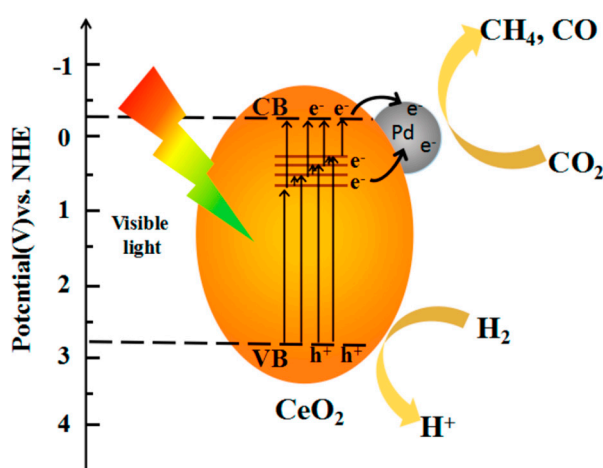


Figure 5. Band energy structure and charge transfer [34]. Copyright 2017 American Chemical Society.

Anandan et al. studied the photodegradation of monocrotophos under visible light irradiation with La-doped TiO_2 . They associated rapid mineralization with the enhanced separation of electrons and holes by doping La^{3+} into the TiO_2 matrix, which subsequently generated a large number of $\bullet\text{OH}$ radicals along with the trapping of excess holes at the surface [35]. In contrast, based on the density functional theory calculation method, Sun et al. worked extensively on the changes of the electronic structure and the photocatalytic activity of TiO_2 after introducing substitutional La dopants. Their calculations demonstrate that the enhanced visible light absorption of La– TiO_2 mainly arises from adsorbed La on the TiO_2 surface rather than from substitutional La doping [36]. Notably, not all kinds of dopants give rise to positive consequences. Chio et al. systematically studied 21 kinds of metal ion-doped TiO_2 materials and their application with respect to various photocatalytic reactions [37]. The results associated with model reactions for the photocatalytic reduction of carbon tetrachloride and the photodegradation of chloroform indicated that only the doping of certain ions, such as Fe^{3+} , Ru^{3+} , Re^{5+} , V^{4+} , and Mo^{5+} , increased reactivity. In addition, the study demonstrated that optimizing the content and placement of the dopant ions content play a positive role in affecting photocatalytic activity. Despite the robust photoactivity of certain metal ion-doped TiO_2 catalysts, some inevitable problems remain and need to be considered. The metal-doped nanomaterials have been shown to suffer from unstable optical properties and thermal instability, in addition to the need to use expensive ion implantation equipment to produce these enhanced materials [38]. Furthermore, the localized *d*-electron state formed in the band gap of TiO_2 may become the recombination center of photogenerated electron–hole pairs, thereby leading to a decline in the photocatalytic activity.

Recently, the non-metal doping of nitrogen (N), sulfur (S), carbon (C), fluorine (F), iodine (I), and phosphorus (P) has been extensively studied due to their relatively high photostability and photoelectric properties [39]. However, in comparison to metal-doped TiO₂, the role of the non-metal dopants as recombination centers of charge carriers might be minimized. By replacing the oxygen atoms in the TiO₂ lattice, the non-metal elements can significantly narrow the bandgap and thereby improve the visible light response of TiO₂. In addition, impurity states can be formed near the valence band edge along with non-metal doping, as displayed in Figure 6. Instead of acting as recombination centers, these occupied levels can be regarded as shallow traps that effectively separate photogenerated electron–hole pairs [40].

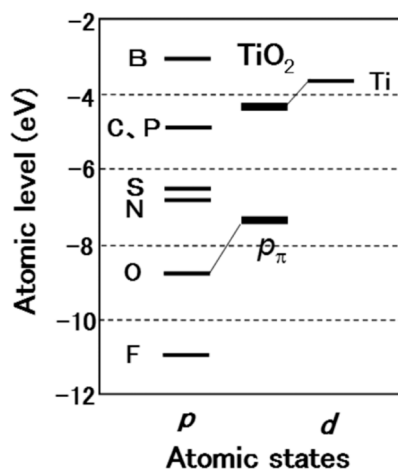


Figure 6. Comparison of atomic p levels among anions. The band gap of TiO₂ is formed between the O 2p π and Ti 3d states [39]. Copyright 2014 American Chemical Society.

In 2001, Asahi et al. first published research on N-doped TiO₂ nanomaterials, which initiated a wave of studies related to non-metal-doped photocatalysts [41]. In a similar work, Zhao et al. reported highly active N-doped TiO₂ nanotubes for CO₂ reduction. Despite the tubular structure with a large surface area providing more surface active sites, the N dopants contributed more to the improved photocatalytic activity. It was found that a redshift of the light absorption and a color center were achieved with N-doped TiO₂ nanotubes because N atoms can substitute for the lattice O atoms of TiO₂, thereby reducing its bandgap and resulting in a ~4 times higher visible light photocatalytic CO₂ reduction activity in comparison to pure TiO₂ nanotubes [42]. Irie et al. prepared C-doped TiO₂ nanoparticles by oxidizing TiC powder, and the efficiency of decomposing gaseous isopropanol under visible light was significantly improved [43]. S-doped anatase TiO₂ with a high surface area was obtained by Li et al. They treated pure TiO₂ using a supercritical strategy and used the materials for methylene blue degradation under visible light irradiation. S atoms with large diameters are difficult to dope into the TiO₂ lattice, but X-ray photoelectron spectroscopy (XPS) detected the existence of S–Ti–O bonds, which introduced lattice defects, acting as shallow traps for electrons and reducing carrier recombination [44]. Li et al. mixed HIO₃ with tetrabutyl titanate and hydrolyzed the samples directly to obtain I-doped TiO₂, which significantly boosted its visible light performance [45].

Although various non-metal ions are used for doping modification of TiO₂, N doping is still one of the most widely used methods to modify the electronic structure and to extend light absorption to the visible range [46]. However, researchers have not yet come to a complete agreement regarding the mechanisms associated with the N doping enhancements. In the literature, it is not difficult to find studies stating that it is not only the dopant concentration but also the dopant location in the TiO₂ lattice (surface or bulk, substitutional, and interstitial) that ultimately determines the photocatalytic properties [17,47]. In the case of N-doped TiO₂ nanomaterials, some researchers believe that only the substitution of O²⁻ by N³⁻ with high dopant concentrations can elevate the valence band edge,

bringing about the desired band gap narrowing [48,49]. However, others suggest that the doping of N will induce oxygen vacancies in TiO_2 and that the enhanced visible light adsorption is associated with the local state induced in the band gap, rather than the generally believed theory that the introduction of N into the TiO_2 lattice can reduce its band gap, as shown in Figure 7 [50].

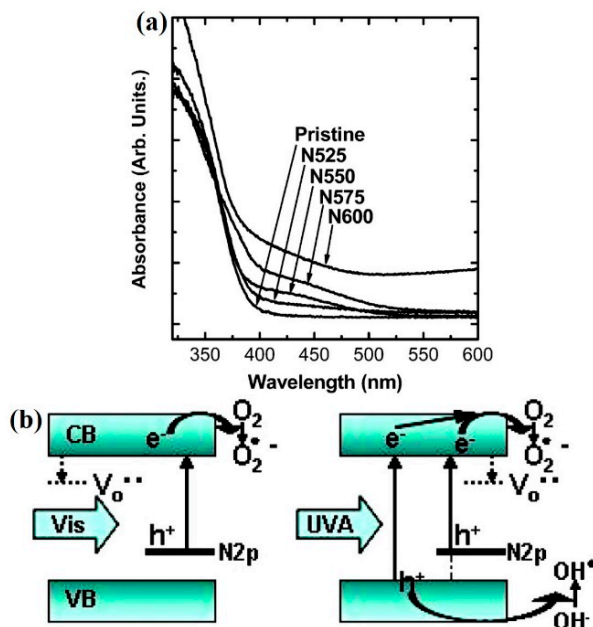


Figure 7. (a) Diffuse reflectance spectra of the anatase TiO_2 nanobelts before and after heat treatment in ammonia gas flow at different temperatures and (b) the band structure of N-doped- TiO_2 under visible and UV light irradiation [50]. Copyright © 2009 American Chemical Society.

As another widely studied non-metal-doped TiO_2 , F-doped TiO_2 also shows promising potential for photocatalytic applications. Zhang et al. obtained F-doped TiO_2 mesocrystals through the topological transformation of TiOF_2 precursors. An in situ characterization technique was adopted to detect the doping process. The results showed that the doping of F was accompanied by the formation of oxygen defects, which ensured a higher visible light response [51]. Park et al. added sodium fluoride to aqueous TiO_2 suspensions to obtain surface fluorinated TiO_2 , and a series of characterizations showed that neither an improvement in crystallinity nor a redshift of the band edge was achieved, but the photocatalytic oxidation of phenol and Acid Orange was considerably enhanced. They attributed such photocatalytic improvement to fluorine surface modification, which enhances free $\bullet\text{OH}$ radical-mediated oxidation pathways [19]. Similar to the doping of N, the reason for the observed high performance upon F doping is still undetermined. Some studies suggest that instead of entering the TiO_2 lattice, fluorine ions adsorbed on the surface of TiO_2 can increase the wettability and surface acidity, which is beneficial to the adsorptivity and e^-/h^+ separation of the oxide [20]. Other researchers hold the opinion that a tail state in the band gap of TiO_2 is formed by F doping, which favors the more efficient utilization of incident light. Recently, an increasing number of studies proposed that a charge compensation effect induced by F doping brings about the formation of a certain amount of oxygen vacancies and Ti^{3+} in TiO_2 , resulting in the enhanced absorption of visible light [52,53]. Although the principle of F doping is not very clear, the proper doping level of F can effectively improve the activity of TiO_2 .

2.2. Intrinsic Defect Formation

In 2011, a black TiO_2 with a narrowed bandgap (approximately 1.5 eV) and fabricated by hydrogenation reduction was reported to achieve absorption of full spectrum sunlight and improved photocatalytic activity [54]. Unsurprisingly, this discovery has aroused worldwide scientific interest

and paved the way towards intrinsic defect modification. Creating intrinsic defects in the TiO_2 lattice is a kind of self-structural modification that includes surface disorder layers, Ti^{3+} /oxygen vacancy self-doping, formation of surface Ti-OH , and incorporation of doped-Consequently, considerable changes in surface properties and electronic and crystal structures are often achieved in this process [55–57]. Furthermore, studies in terms of defect engineered TiO_2 have confirmed that these intrinsic defects are emerging as a promising attribute for improving the separation of electrons and holes, outperforming, in some cases, other kinds of modified TiO_2 nanomaterials [58].

Since the study by Chen et al., various methods have been developed to induce defects in TiO_2 , including direct reduction of TiO_2 ; that is, the currently reported H_2 , Al, Na, Mg, NaBH_4 , hydrides, imidazoles, etc. can effectively transfer modify pure TiO_2 nanomaterials into their defect engineered counterparts under certain conditions [59,60]. In addition, electrochemical reduction and high-energy particle bombardment (such as photon beam and H_2 plasma or electron beam) are widely used to induce TiO_2 defects. Partial oxidation from low-valence-state Ti species such as TiH_2 , TiO , TiCl_3 , TiN , and even Ti foil represents another promising approach, fulfilling the needs for highly active TiO_{2-x} photocatalysts [61]. Liu et al. prepared rice-shaped Ti^{3+} self-doped TiO_{2-x} nanoparticles through mild hydrothermal treatment of TiH_2 in H_2O_2 aqueous solution, and proposed a unique “surface oxide-interface diffusion–redox mechanism” (as shown in Figure 8) to explain the formation process of TiO_{2-x} [62]. The defect types and their formation mechanism in TiO_{2-x} are closely related to the preparation methods. Generally, the Ti-H bond is present only in hydrogen-reduced TiO_{2-x} , while the surface disorder layer causes severe damage to the TiO_2 structure. Thus, relatively strong reduction conditions are required, such as high temperature/pressure hydrogen reduction, aluminothermic reduction, hydrogen plasma treatment, etc. Surface Ti-OH , Ti^{3+} , and oxygen vacancies commonly exist in most defective TiO_2 nanostructures [63].

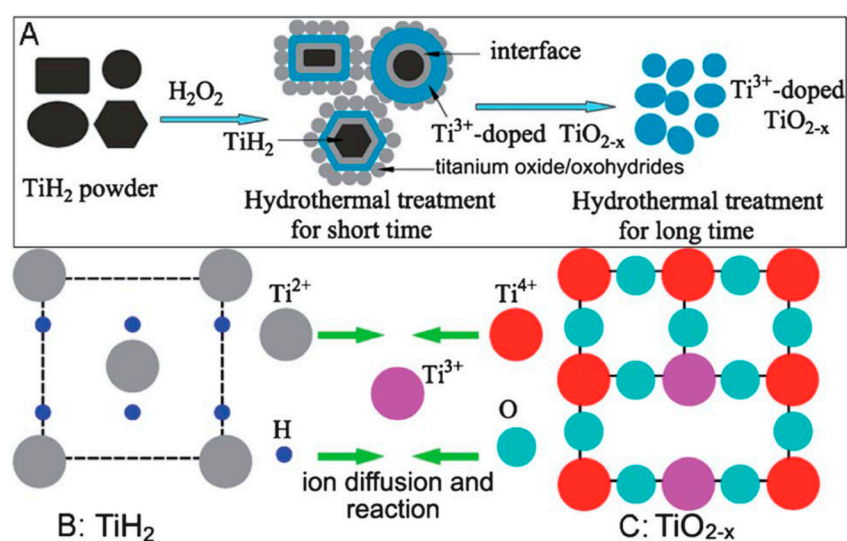


Figure 8. (A) Schematic of the formation mechanisms for the rice-shaped Ti^{3+} self-doped TiO_{2-x} nanoparticles. (B,C) The interface diffusion–redox diagram. The green arrows indicate ion diffusion [62]. Copyrighted 2014 The Royal Society of Chemistry.

The dominant mechanism involved in improving photocatalytic performance by inducing intrinsic defects into TiO_2 can be explained, both experimentally and theoretically, to be the regulation of the band structure of TiO_2 and boosted charge separation and transport. For black TiO_2 , band tail states and shallow dopant states can be formed to reduce its band gap and further increase its optical absorption properties. Chen et al. observed a disordered surface layer in black TiO_2 nanocrystals after a hydrogenation treatment, as shown in Figure 9. From the high-resolution transmission electron microscopy (HRTEM) spectra, it can be readily observed that the straight lattice fringes are bent at the edge of the particles, and the lattice spacing is no longer uniform, indicating that the hydrotreated

black TiO₂ nanoparticles possess a “crystal-disordered” core-shell structure. Such a disordered layer is believed to facilitate the introduction of the tail state at the top of the valence band and the bottom of the conduction band, consequently yielding a redshift of the light absorption [54]. Moreover, because the disorder layer exhibits a set of properties that are distinct from those of their crystalline counterparts, rapid charge separation could be realized when the amorphous layer closely contacts crystalline TiO₂. The lattice distortions tend to blueshift the VBM while having less impact on CBM. Therefore, the photogenerated holes accumulate in the thin disordered shell and participate in the photocatalytic reactions immediately; electrons are widely spread in both the shell and core regions. This result highlights the strong synergistic effect on charge transfer between the crystalline and disordered parts [64].

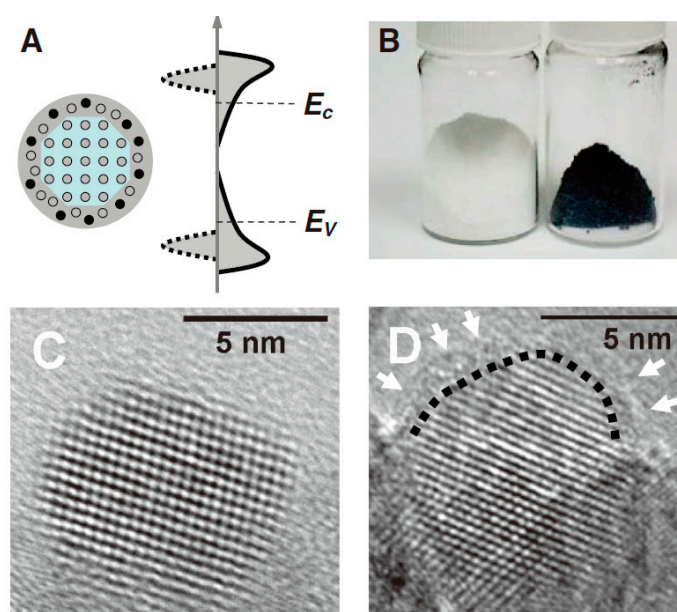


Figure 9. (A) Schematic illustration of the structure and electronic DOS of a semiconductor in the form of a disorder-engineered nanocrystal with dopant incorporation. (B) A photo comparing unmodified white and disorder-engineered black TiO₂ nanocrystals. (C,D) HRTEM images of TiO₂ nanocrystals before and after hydrogenation, respectively [54]. Copyright 2011 American Association for the Advancement of Science.

For Ti³⁺/oxygen vacancy incorporation and H-doping in reduced TiO_{2-x}, the hybridization of Ti-3d, O-2p and H-1s orbitals results in the mid-gap states formation below the CBM and the Fermi level's upshift [65,66]. The extra electrons in either Ti³⁺ or oxygen vacancies are inclined to occupy the empty states of Ti ions, forming new Ti 3d bands below the CBM. With a further increase in defect concentration, the 3d band shifts deeper and finally results in multiple bands in the CBM. Moreover, the existence of multiple mid-gap states as well as the associated derivative (surface Ti-OH) can also function as extra carrier trap sites or carrier scavengers to prolong the lifetime of electrons and holes [67]. The high concentration of electron donors will greatly improve the conductivity of materials and promote the transfer of carriers [68]. Wang et al. treated pure white TiO₂ with hydrogen plasma to fabricate H-doped black TiO₂ for photodegradation of methyl orange under visible light irradiation. The as-prepared samples showed a degradation rate 2.5 times that of the white counterpart [69]. Sinhamahapatra et al. reported a novel controlled magnesiothermic reduction to synthesize reduced TiO_{2-x} under 5% H₂/Ar atmosphere [70]. During this process, the band position and band gap, surface defects and oxygen vacancies can be well regulated to maximize the optical adsorption in the visible and infrared regions and minimize the charge recombination centers. As shown in Figure 10, a new controlled magnesium thermal reduction method to synthesize and reduce black TiO₂ under 5% H₂/Ar atmosphere. The material has the best band gap and band position, oxygen vacancy, surface

defect, and charge recombination center, and the optical absorption in visible and infrared regions is improved obviously. These synergistic effects enable the defective TiO_{2-x} with Pt as a co-catalyst to produce H_2 at a rate of $43 \text{ mmol h}^{-1} \text{ g}^{-1}$ under the full solar wavelength light illumination, superior to other reported photocatalysts for hydrogen production.

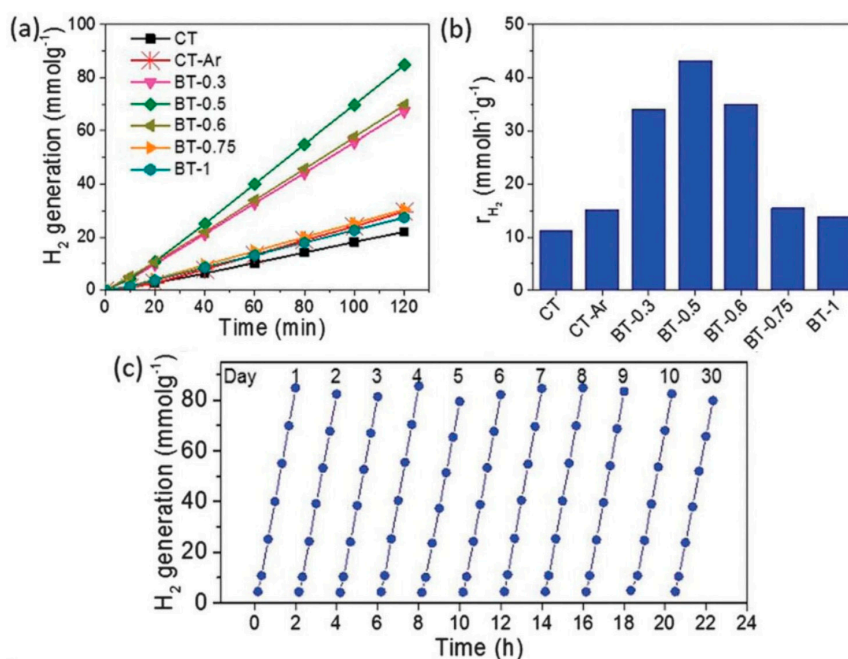


Figure 10. (a) H_2 generation profile, (b) rate (r_{H_2}) of hydrogen generation for different samples, and (c) the stability study of the sample BT-0.5 under the full solar wavelength range of light [70]. Copyright 2015 The Royal Society of Chemistry.

To date, numerous strategies, either common or uncommon, have been developed to introduce various kinds of dopants or defects into the TiO_2 matrix. However, considering its highly stable nature, most methods are rigorous and energy-consuming, and are contrary to the sustainable and environmentally friendly development criteria. Therefore, an increasing number of studies are dedicated to seek convenient, economical, energy efficient, and environmentally friendly methods for the structural modification of TiO_2 [71]. In our recent studies, we developed a facile photoreduction strategy to induce intrinsic defects into anatase TiO_2 to modulate its band structure, thereby extending the absorption of incident light to the visible region. As shown in Figure 11, the band gap was narrowed to 2.7 eV, and the color changed to earth yellow after the photoreduction treatment. NH_4TiOF_3 mesocrystals were adopted as precursors, which can release fluorine and nitrogen ions during the topological transformation process. Thus, non-metal ion doping (i.e., F and N ions) was also achieved simultaneously, further improving the transport and separation of photogenerated charge carriers. The as-prepared NF- TiO_{2-x} exhibited excellent photocatalytic degradation and photoelectrochemical efficiency under visible light irradiation compared to pristine TiO_2 [72,73].

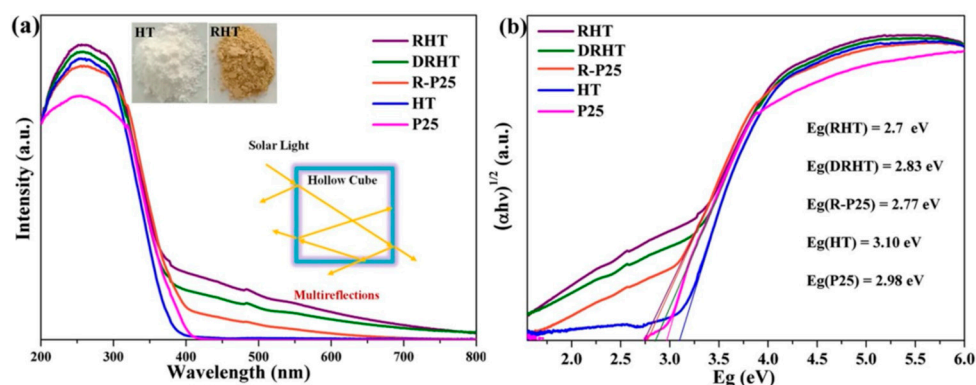


Figure 11. (a) UV-Vis diffuse reflectance spectra and (b) Tauc plot for band gap determination [73]. Copyright 2018 Springer Nature Publishing AG.

3. Morphology Modification

It is well known that the photocatalytic performance of semiconductors is closely related to their structural and morphological characteristics at the nanoscale, including their size, dimensionality, pore structure and volume, specific surface area, exposed surface facets, and crystalline phase content [74]. During the past few decades, numerous promising structure engineering strategies have been developed to fabricate highly active photocatalysts with the desired morphology and structure. Among them, particular emphasis has been placed on controlling and optimizing the structural dimensionality of a given semiconductor to improve its photocatalytic efficiency.

Zero-dimensional TiO₂ nanospheres are the most widely studied TiO₂-based materials because of their high specific surface area and attractive pore structures [75–77]. Figure 12 shows a classic ripening approach to synthesize hollow nanospheres [75]. As photocatalytic reactions take place on the surface of the photocatalyst, TiO₂ nanoparticles with smaller sizes are inclined to provide more reactive sites, resulting in better photocatalytic performance. Moreover, due to the quantum size effect, the photogenerated electrons and holes in the bulk regions are able to migrate to the surface of TiO₂ nanoparticles via shorter distances, thereby considerably reducing the carrier quench rate [78]. TiO₂ nanospheres are also good candidates as light captors, and their structural features enable as much light as possible to access the interior, resulting in amazing light harvesting capabilities. However, it should be mentioned that the diffusion length of photogenerated electrons and holes must be longer than the particle size to avoid the recombination of the dominant carriers on the surface of the photocatalyst, which is very important for achieving efficient charge carrier dynamics [79].

One-dimensional (1D) nanostructures, including nanotube (NT), nanorod (NR), nanobelt (NB), and nanowire (NW), have become a popular research topic in recent years. They have been extensively studied because of their distinct optical, electronic and chemical properties. Despite some similar features with nanoparticles, such as quantum confinement effects and large surface area, 1D nanomaterials possess many unique properties, which are hard for other categories of structured materials to achieve. For example, 1D nanostructures restrict the migration of electrons and protons by allowing the lateral confinement of electrons/protons and guide their transport in the axial direction [80,81]. Furthermore, excellent flexibility and mechanical properties enable them to be easily used and recycled. In this regard, 1D TiO₂-ordered nanostructures are promising not only for constructing highly active photocatalytic systems but also for building blocks for various (photo)electrochemical devices, such as batteries, fuel cells, solar cells, and photoelectrochemical cells. To further optimize the photocatalytic reactivity of 1D TiO₂ nanomaterials, one can precisely regulate the aspect ratio (the ratio of length to diameter) or modify these 1D nanostructures with novel strategies to accelerate electron transport and separation processes, as well as to enhance the capture of incident light; TiO₂ nanotubes are examples of these materials [82]. Through the electrochemical anodization process, it is possible to precisely control the tube crystal structure

(anatase, rutile, or amorphous) and tube geometry (diameter and length), as shown in Figure 13a, or direct the tube arrangements to obtain a defined tube-to-tube interspace (Figure 13b). For the sake of extending the scope of application, constructing flow through membranes with TiO₂ nanotubes is a good choice (Figure 13c). Other modifications for minimizing charge carrier annihilation and boosting light harvesting are illustrated in Figure 13d–i, ranging from self-decoration to surface alterations to energy band engineering.

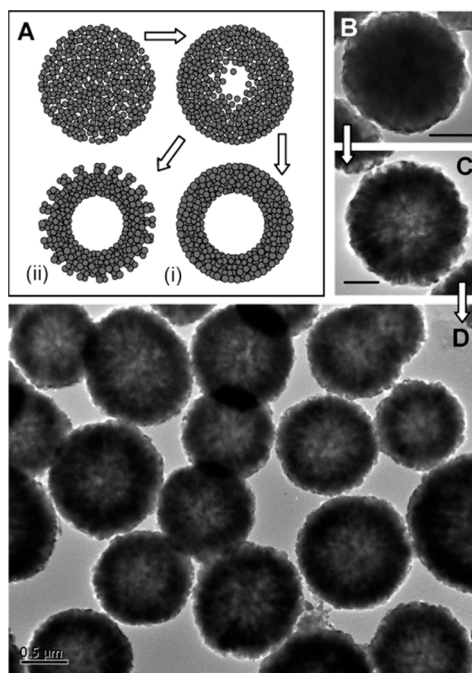


Figure 12. (A) Schematic illustration (cross-sectional views) of the ripening process and two types (i and ii) of hollow structures. Evolution (TEM images) of TiO₂ nanospheres synthesized with 30 mL of TiF₄ (1.33 mM) at 180 °C with different reaction times: (B) 2 h (scale bar = 200 nm), (C) 20 h (scale bar = 200 nm), and (D) 50 h (scale bar = 500 nm) [75]. Copyright 2004 American Chemical Society.

TiO₂ nanosheets, nanoflakes, and thin films consist of titania-based two-dimensional nanomaterials, which have flat surfaces and high aspect ratios. The lateral size of some nanomaterials is controllable, ranging from the sub-micrometer or even nanometer level to several tens of micrometers with thicknesses of 1–10 nm. Such structures provide TiO₂ nanomaterials with several unique characteristics, such as excellent adhesion to substrates, low turbidity and high smoothness [83]. Furthermore, when exposed to UV light irradiation, TiO₂ 2D nanomaterials exhibit superhydrophilicity, which leads to a variety of potential applications, such as self-cleaning coatings and electrodes in photoelectronic devices [84]. Notably, considering that photocatalytic reactions always occur on the surface of catalysts, the exposed crystal facets are of great importance in determining the photocatalytic performance. Accordingly, developing TiO₂ crystals with different active facets is highly desirable in many applications. In general, TiO₂ nanocrystals have three basic low-index exposed facets—{101}, {001}, and {010}—with surface energy relationships of {001}, $0.90 \text{ J m}^{-2} > \{100\}$, $0.53 \text{ J m}^{-2} > \{101\}$, 0.44 J m^{-2} [85,86]. Therefore, as the most thermodynamically stable facets, the {001} crystal facet is dominant among most anatase TiO₂ nanomaterials, reducing the overall surface energy of the material. In 2008, Yang et al. first reported TiO₂ single crystals with 47% highly active {001} facets exposed to HF as capping agents [87]. This work has attracted considerable global attention. Since then, TiO₂ with various ratios of exposed {001} facets have been successfully fabricated [88]. Meanwhile, other active planes, such as {010}, {111}, and {110}, have also been reported and widely used in water splitting, solar cells, artificial light synthesis and other fields, as shown in Figure 14 [89]. Zheng et al. obtained {001} facet-oriented anatase by facile heat treatment of a tetrabutyl titanate, absolute ethanol, and HF mixture.

Such a material with 85% {001} facets exhibited much higher photocatalytic activity in comparison to commercial P25 materials [90].

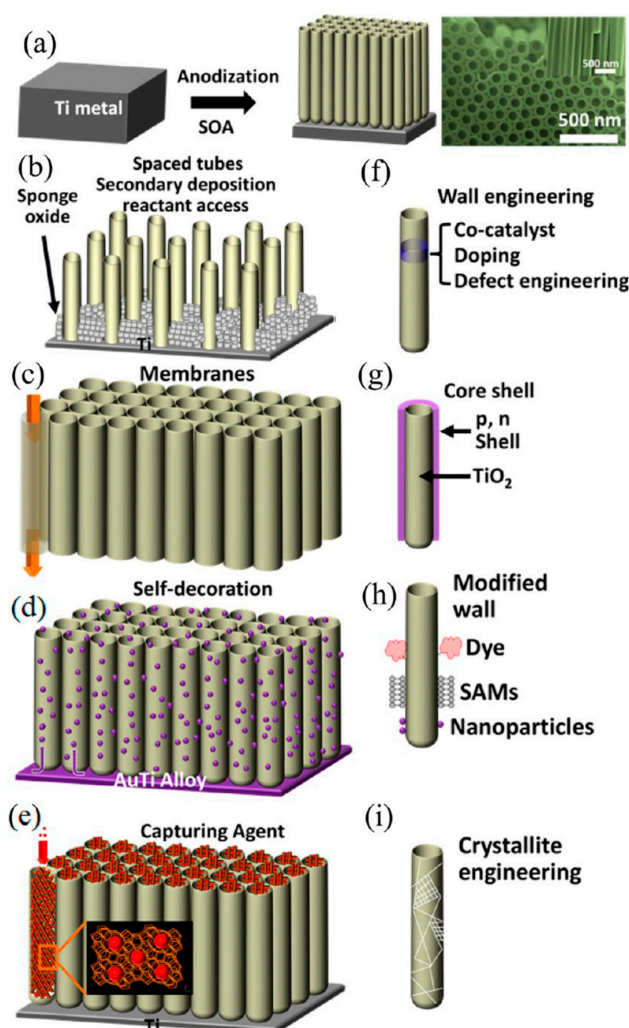


Figure 13. Schematic drawing of (a,b) formation and (c–i) modification of anodic nanotube arrays (as discussed in the text) [82]. Copyright 2017 American Chemical Society.

During the process of photocatalytic reactions, oxidation predominantly occurs in the {001} facets, while reduction occurs in the {101} crystal plane of TiO₂ because the {101} facet (with relatively low surface energy) tends to attract more electrons. Electron holes subsequently accumulate in the {001} plane, facilitating the space separation of electron–hole pairs [91]. In addition, Ti atoms of the {001} plane exist mainly in the form of 5-coordination, which can provide more active sites that more readily attract free reactant molecules than the {101} plane. Thus, when a certain proportion of {001} crystal facets are exposed, the photocatalytic activity increases rapidly. Nevertheless, it is not always the case that a higher {001} crystal face exposure ratio results in improved catalytic performance. Studies have reported that the photocatalytic activity is compromised when the proportion of {001} facets exceeds 71% [89]. In addition, faceted TiO₂ photocatalysts suffer from weak visible light utilization due to their large band gap. Hence, the modification of the electronic structure of faceted TiO₂ to fully utilize sunlight and promote the migration and separation of electron/hole pairs is highly desirable. Wang et al. prepared Ti³⁺ self-doped TiO₂ mesoporous nanosheets dominated by {001} facets with supercritical technology. They associated the extended region of incident light absorption with the introduction of Ti³⁺ [91]. Using an ionic liquid as a surface control agent, Biplab et al.

synthesized microporous TiO₂ nanocrystals with exposed {001} facets. After depositing Pt on the surface, the hydrogen production rate in visible irradiation was greatly improved [92].



Figure 14. Summary of main shapes and applications (i.e., lithium ion batteries, photocatalytic hydrogen evolution, photodegradation, and solar cells) of anatase, rutile, and brookite TiO₂ crystals with their surfaces consisting of different Facets [89]. Copyright 2014 American Chemical Society.

A three-dimensional TiO₂ hierarchical structure based on intrinsic shape-dependent properties has been the central focus of many recent studies. Designed and fabricated 3D TiO₂ nanomaterials commonly incorporate interconnected structures, hollow structures and hierarchical superstructures constructed from small dimensional building blocks [93]. Most of these novel structures include larger spatial dimensions and more varied morphologies. The high surface-to-volume ratio provides a more efficient diffusion path for reactant molecules, enabling the contaminant molecules to enter the framework of the photocatalyst for efficient purification, separation, and storage. In addition, the unique optical characteristic is of particular interest because many of these architectures have distinctive physicochemical properties favorable for incident light utilization. For example, when light is irradiated onto the surface of the TiO₂ hierarchical structure, photons are scattered multiple times, so the probability of the catalyst absorbing photons is increased; this phenomenon is known as the “trapping effect” and is illustrated in Figure 15 [94].

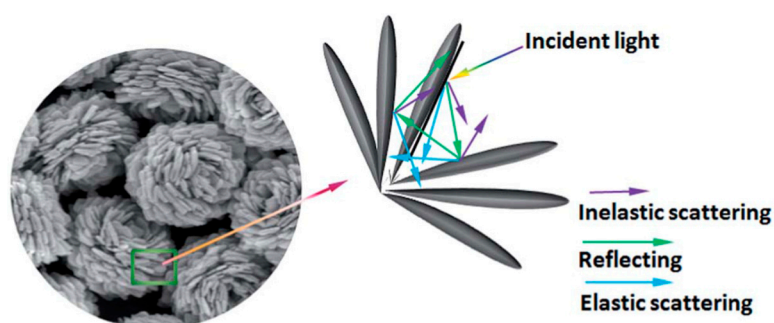


Figure 15. Schematic diagram of the reflecting and scattering effects in hierarchical microspheres [94]. Copyright 2014 The Royal Society of Chemistry.

The hollow structure TiO₂ nanomaterials have attracted considerable attention due to their amazing light harvesting ability, low density, and large specific surface area. The hollow structure, on the one hand, is capable of providing a large amount of space to accommodate more reactant molecules, thereby increasing the effective contact between the catalyst and the reactants. On the other hand, incident light inside the cavity can undergo multiple reflections to capture more light, as shown in Figure 16 [95]. Kondo et al. obtained TiO₂ hollow nanospheres through hydrothermal and calcination processes with polymer polyethylene cationic balls as templates. The as-prepared photocatalyst had more favorable activity than its commercial counterparts with respect to decomposing isopropanol [96]. In the following work, an ultrathin TiO₂ shell-like structure was prepared in a similar manner with a shell thickness of approximately 5 nm. The morphology of the TiO₂ hollow materials prepared by the hard template method is relatively uniform, and the composition and thickness of the shells are adjustable. However, the preparation process is complicated and requires multiple execution steps to be realized. Moreover, the hollow structure may be destroyed when the template is removed. Therefore, alternative strategies, including soft templates and non-template methods, have played an increasingly important role in the development of hollow structure TiO₂ nanomaterials in recent years.

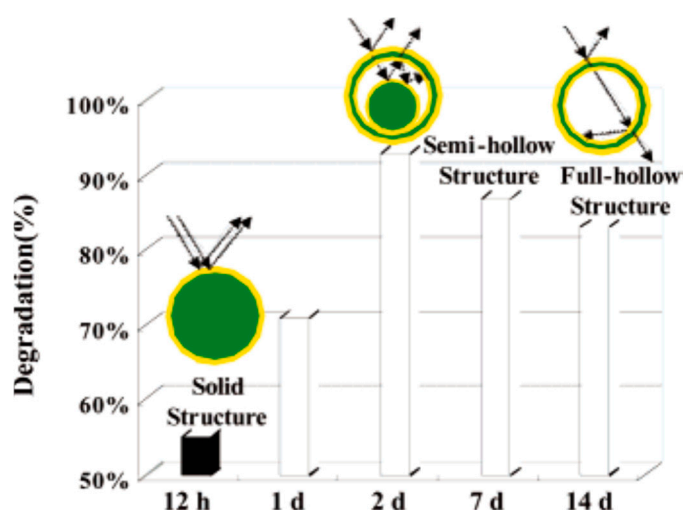


Figure 16. Comparison of photocatalytic activities of titania spheres with solid, sphere-in-sphere, and hollow structures [95]. Copyright 2007 American Chemical Society.

Li et al. prepared hollow TiO₂ nanospheres with high photocatalytic activity by a template-free process. The increased catalytic activity is mainly due to the multiple reflections of incident light inside the TiO₂ sphere, which extends the optical path [97]. Multichannel TiO₂ hollow nanofibers were constructed by Zhao et al. for degrading gaseous acetaldehyde, and the specific surface area of this material increased rapidly as the number of channels increased. They proposed that the multichannel hollow structures induced both an inner trap effect on gaseous molecules and a multiple-reflection effect on incident light, which were the main reasons for the improved photocatalytic activity of TiO₂ hollow fibers [98]. Shang et al. synthesized submicron-sized TiO₂ hollow spheres from a mixture of TiCl₄, alcohols, and acetone by a template-free solvothermal method. Control of the sphere size was achieved by adjusting the ratio of ethanol to acetone. Based on a series of characterizations, they suggested a possible formation mechanism for the hollow structure: the tiny anatase phase TiO₂ nanoparticles with poor crystallinity form through a hydrolysis reaction, due to the very high surface energy, and then quickly aggregate to form spheres. The increased water promotes the crystallinity of particles in the spherical shell, while the internal particles dissolve and migrate to the spherical shell, leading to the formation of highly crystalline TiO₂ hollow spheres [99]. An intriguing work carried out by Kang et al. to establish hierarchical anatase TiO₂ nanocubes with hollow structures has been reported recently. Instead of seeking complicated templates or surfactants, they directly

converted NH_4TiOF_3 mesocrystals to hollow spiny TiO_2 with a high specific area and photodegradation activity [73].

4. TiO_2 Mesocrystals

It is widely accepted that for TiO_2 -based photocatalytic materials, large crystallites result in high structural coherence, which benefits the transfer and separation of electron–hole pair, while the availability of plentiful reaction sites is dependent on obtaining large specific surface areas. However, producing a structure that simultaneously satisfies the requirements of large crystallites and high surface area is extremely challenging. Fortunately, the advent of mesocrystals is a promising material that may meet the challenge [100]. Mesocrystals were first proposed by Cölfen and Antonietti in 2005, and since then have received increased attention [101]. Different from the classical single crystals in which the crystal lattice of the entire sample is continuous with no grain boundaries and polycrystals whose units do not have the same orientation, mesocrystals are a new kind of superstructure material that follow a nonclassical crystallization process involving crystallographically ordered assemblies of nanocrystal building blocks. The relevant formation mechanisms of TiO_2 mesocrystals reported thus far mainly include topotactic transformation, mineral bridges, nanoparticle alignment with organic matrices, physical ordering, space constraints, and self-similar growth [100]. Different methods may give rise to different structures and morphologies, but the as-prepared TiO_2 mesocrystals are usually single-crystal-like structures with high porosity, surface area, and crystallinity; they are considered periodically hierarchical structures that are similar to sophisticated biominerals. All of these features pave the way for a wide range of applications, such as catalysis and energy storage and conversion [102].

Fabrication and modification strategies for TiO_2 mesocrystals have developed rapidly in recent years. Due to the similar structure between NH_4TiOF_3 and TiO_2 , preparing TiO_2 mesocrystals through topotactic transformation from NH_4TiOF_3 represents an innovative process. As illustrated in Figure 17, the critical parameters in the {001} facets of both NH_4TiOF_3 and TiO_2 are quite similar, with an average lattice mismatch of 0.02%. The position of titanium atoms in the {001} plane of TiO_2 is similar to NH_4TiOF_3 , but in NH_4TiOF_3 , these are separated by ammonium ions in a lamellar structure. Hence, it is reasonable to use NH_4TiOF_3 as a starting material, transforming it into TiO_2 mesocrystals by thermal decomposition or aqueous hydrolysis with H_3BO_3 [71].

Based on this mechanism, Majima et al. performed extensive studies on tailoring TiO_2 mesocrystals with versatile structures and morphologies, as well as postmodifications to further improve their photocatalytic efficiency. For example, to investigate the anisotropic electron flow in different facets and to maximize their separation during the photocatalytic reaction, Zhang et al. controllably synthesized a specific facet-dominated TiO_2 superstructure with NH_4F as an orientation-directing agent [103]. Under UV light irradiation, mesocrystals with different facet ratios showed different reactivity orders in the photooxidation of 4-chlorophenol, i.e., {001} > {101} (by 1.7 times), and photoreduction, i.e., {101} > {001} (by 2–3 times).

Moreover, constructing the composite of MoS_2 and TiO_2 mesocrystals, as well as the co-catalyst selective modification on TiO_2 , also showed the desired separation of photogenerated charge carriers during the hydrogen evolution reaction [104]. In terms of extending the absorption of incident light to the visible region, Zhang et al. tried doping or codoping non-metal elements into the TiO_2 matrix to examine the effects on its electronic structure and band gap. An in situ fluorine-doped TiO_2 superstructure was recently realized. F doping into TiO_2 mesocrystals for the incorporation of active color centers facilitates visible light harvesting and accelerates charge separation for hydrogen generation [51]. They further introduced nitrogen and fluorine codopants into {001} facet-oriented TiO_2 mesocrystals during topochemical transformation for photoreduction of Cr(VI) under visible light illumination. The extended optical light absorption could be attributed to doped nitrogen, which introduces the isolated mid-gap state. The high yield of hydroxyl radicals and preferential adsorption are correlated with fluorine doping, as confirmed by the comparison between untreated TiO_2 with

TiO₂ washed in NaOH aqueous solution. The synergistic effect on charge separation and trapping was suggested through a femtosecond time-resolved diffused reflectance (TDR) measurement [105]. As shown in Figure 18, the g-C₃N₄ nanosheet/TiO₂ mesocrystal metal-free composite was successfully constructed by Elbanna et al. [106]. The as-prepared sample exhibited an excellent hydrogen evolution rate under visible light irradiation without any noble metal co-catalyst. Then, they further broadened the light capture of the TiO₂ mesocrystals to include near-infrared regions. Au nanorods (NRs) with various aspect ratios were loaded onto the surface of TiO₂ by the ligand exchange method. Different aspect ratios resulted in different incident light absorption and photogenerated electron transfer. The highest photocatalytic activity of Au NRs and TMC composites reached 924 μmol h⁻¹ g⁻¹ under visible-near-infrared (NIR) light irradiation [107].

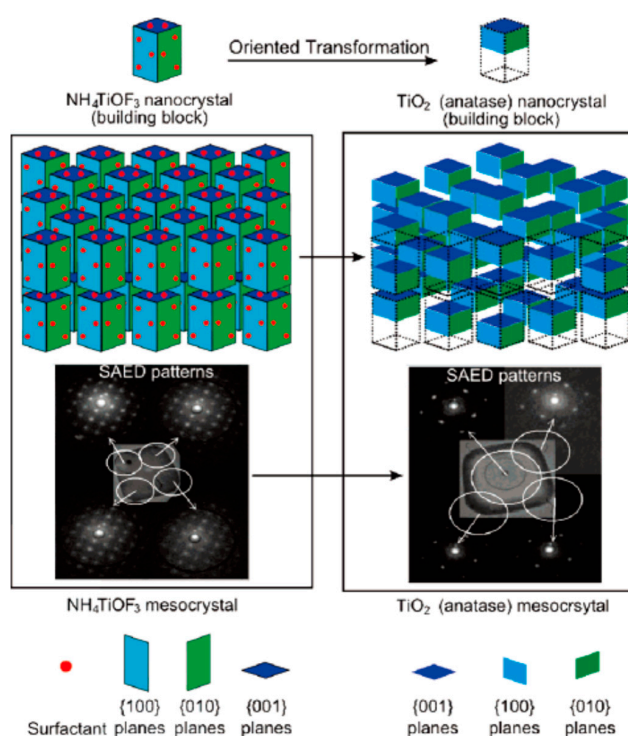


Figure 17. Illustration of the oriented transformation of NH₄TiOF₃ mesophyte to TiO₂ (anatase) mesocrystal [71]. Copyright 2008 American Chemical Society.

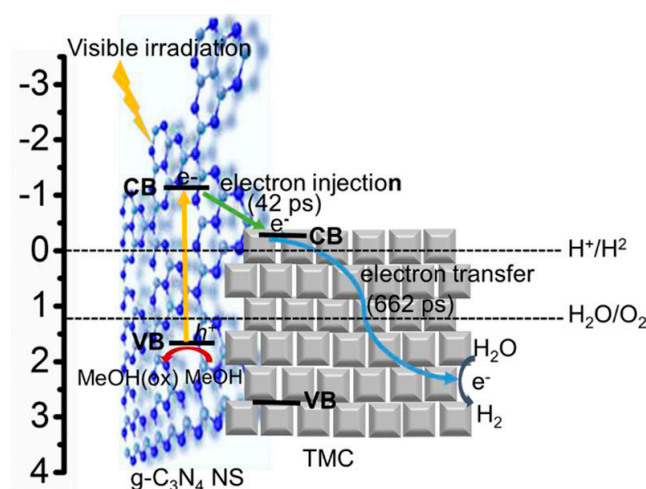


Figure 18. Representative scheme of electron injection and movement in g-C₃N₄ NS (31 wt %)/TMC during visible-light irradiation [106]. Copyright 2017 American Chemical Society.

Considering the aforementioned merits of mesocrystal nanomaterials, we recently tried different approaches to further improve the optical absorption properties of TiO_2 mesocrystals, in addition to their enhanced transfer and separation properties. Oxygen vacancies and N dopants were successfully introduced into the TiO_2 lattice with a facile low temperature calcination process [108], as shown in Figure 19. NH_4TiOF_3 mesocrystal nanocubes were used as precursors in our system, and topological transformation from NH_4TiOF_3 to TiO_2 facilitated the release and doping of nitrogen. Oxygen vacancies were also readily produced in the inert heating atmosphere. The significantly improved photodegradation and photoelectrochemical performance under visible light irradiation may be associated with the unique structure of mesocrystals as well as the introduction of foreign and intrinsic defects.

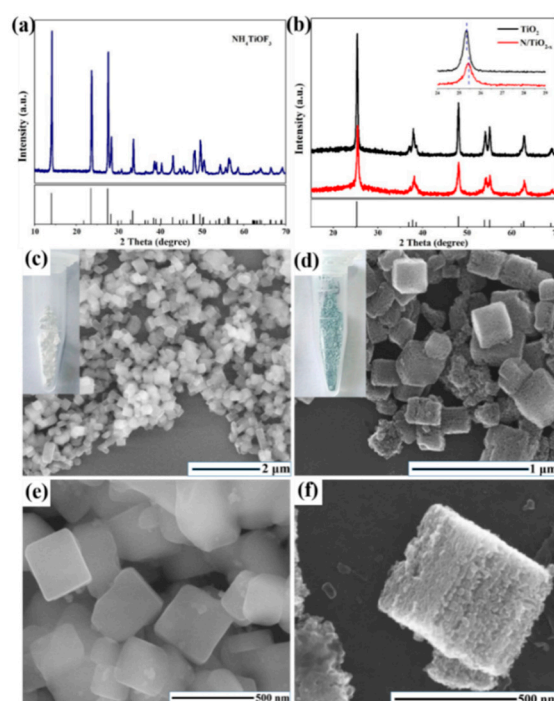


Figure 19. Schematic representation of the synthesis of TiO_x nanosheets. X-ray powder diffraction (XRD) pattern of (a) NH_4TiOF_3 and (b) $\text{N}/\text{TiO}_{2-x}$. SEM images of (c,e) NH_4TiOF_3 and (d,f) $\text{N}/\text{TiO}_{2-x}$ [108]. Copyright 2019 The Royal Society of Chemistry.

5. Separation of Charges

Since metals and metal oxides have different working functions, resulting in the formation of a Schottky potential barrier, an effective modification method is to deposit precious metals (Ag, Au, or Pt) on the surface of metal oxides.

Choi et al. presented Ag/TiO_2 by a photodeposition method [109]. Due to the different transfer rates of interface charges between electrons and holes to redox species in water, excessive charges can accumulate on photocatalysts [110,111]. By depositing Ag, which can provide a temporary home for excessive electrons, the composite utilized the electron storage capacity to promote the separation of electrons and holes to reduce $\text{Cr}(\text{VI})$ in the following dark period. Li et al. prepared a sandwich structure with $\text{CdS}-\text{Au}-\text{TiO}_2$ on a fluorine-doped tin oxide (FTO) substrate [112]. In this composite structure, Au nanoparticles not only acted as an electronic relay between CdS quantum dots (QDs) and TiO_2 to increase charge separation occurring on a long-time scale but also served as a plasma photosensitizer that prolonged the photoconversion to improve the absorption range of light. The rate of charge transfer and reverse transfer depends on the relative energy of the hot plasma electrons to the Schottky barrier [112]. The PEC performance is represented in Figure 20.

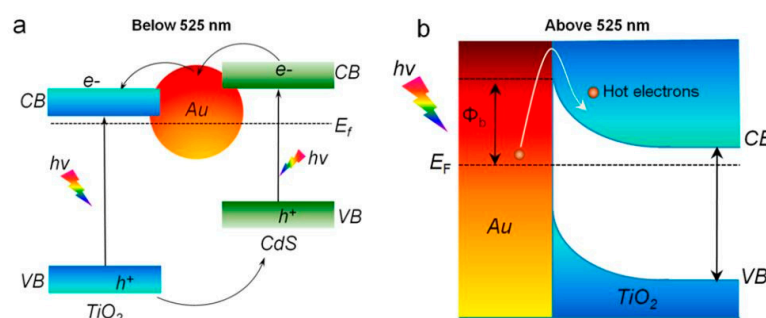


Figure 20. (a) Electron relay effect of Au nanoparticles, facilitating the charge transfer from CdS QDs to TiO₂ nanorods under the irradiation of incident solar light with a wavelength <525 nm. (b) Plasmonic energy transfer from the excited Au nanoparticles to TiO₂ through hot electron transfer under the irradiation of incident solar light with a wavelength >525 nm. CB = conduction band, VB = valence band, E_F = Fermi energy level, and Φ_b = Schottky barrier [112]. Copyright 2014 American Chemical Society.

Precious metal deposition can greatly improve the performance of catalysts, but the scarcity of precious metals dramatically limits this modification method and makes it difficult to achieve industrial-scale production. In this case, the search for an inexpensive and efficient doped composite has also attracted much attention. Carbon, abundant on earth, has good electrical conductivity, and its combination with TiO₂ can result in excellent photocatalytic performance. Wang et al. demonstrated TiO₂–carbon nanoparticles by the sol–gel method and then synthesized core–shell-structured TiO₂ and amorphous carbon [113]. This unique morphology and structure result in the modified TiO₂ sample exhibiting enhanced responsiveness and excellent photocatalytic activity. Due to the rapid charge transfer in the carbon shell, both the carrier separation efficiency and the photodegradation of pollutants in water is improved. The reduced TiO₂ is also more efficient in the production of H₂ due to its correct edge position.

6. Application of TiO₂ Nanomaterials

Over the past several years, semiconductors, especially titanium dioxide, have been widely used as photocatalysts. It is well known that there are three main steps associated with the photocatalysis process: (1) generation of electrons and holes after the absorption of photons; (2) separation and migration of the charge; and (3) transition of the charge and reaction between the carriers and the reagent. To date, TiO₂ has been mainly applied in the areas of environmental conservation, new energy resources, and so on. In this section, we will focus on recent progress in these photocatalytic applications of TiO₂.

6.1. Applications in the Environment

6.1.1. Degradation of Aqueous Pollutants

Industrial development is often accompanied by pollution of the environment, especially water. Photocatalytic water treatment using heterogeneous semiconductors under visible light is considered an eco-friendly technology. Photocatalysis involves the generation of large numbers of electrons and holes on the surface of TiO₂ after the absorption of photons; the photogenerated holes have considerable oxidizing capacity and can degrade almost all organic contaminants including carbon dioxide (CO₂). However, due to its own deficiencies, such as a wide bandgap and fast recombination of electrons and holes, TiO₂ cannot make full use of sunlight to remove the pollutants in water. Wang et al. reported hydrogenation by TiO₂ nanosheets with exposed {001} facets maintained by the formation of Ti–H bonds [114]. By annealing the fine-sized pristine hydrothermal product under a high-pressure hydrogen atmosphere, the hydrogenation of F-modified anatase TiO₂ nanosheets (with exposed high

percentages of {001} facets) was achieved. Under UV–Vis and visible light irradiation, this material decomposed methylene blue (MB) faster than P25 and pristine TiO₂, as shown in Figure 21.

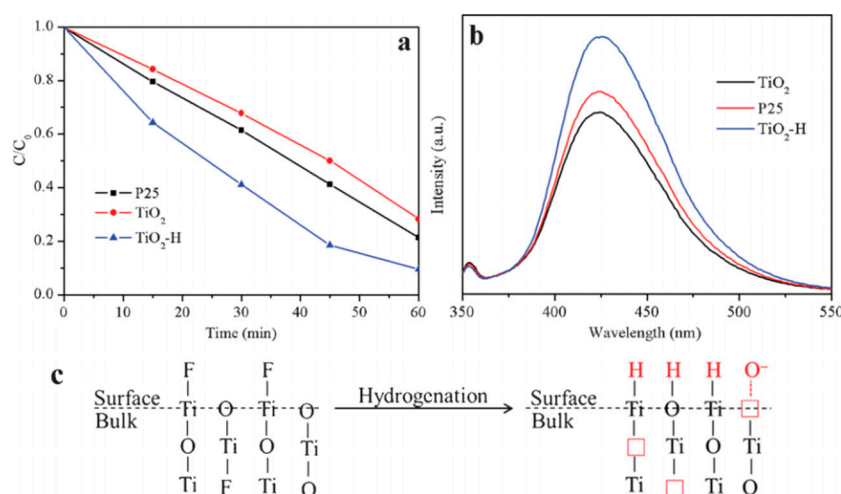


Figure 21. Photocatalytic decomposition of MB (a) and •OH generation measurement (b) of TiO₂ and TiO₂-H under UV–Vis light irradiation. Schematic illustration (c) of the hydrogenation effect on the structural change in TiO₂ and TiO₂-H [114]. Copyright 2012 The Royal Society of Chemistry.

Plodinec et al. applied black TiO₂ nanotube arrays with Ag nanoparticles, which promoted hydrogenation for the degradation of salicylic acid [115]. The photocatalyst can degrade salicylic acid effectively, and its photocatalytic performance far exceeds that of TiO₂ nanotubes and commercial TiO₂ P25 (the reference material used for the modeling of photocatalytic processes). Ling et al. prepared TiO₂ nanoparticles (with diameters of 10–23 nm) that exhibited photocatalytic activity [116]. The initial degradation rate of phenol by a TiO₂ nanocatalyst was 6 times higher than that achieved with H₂O₂ alone, and the addition of H₂O₂ to TiO₂ can increase the initial concentration of hydroxyl radicals and accelerate the degradation rate. Hao et al. developed a TiO₂/WO₃/GO nanocomposite (via a hydrothermal synthesis), which presented excellent optical absorbance and displayed excellent photocatalytic activity for the degradation of bisphenol A [117].

In addition to the oxidizing capacity, the photogenerated electrons on TiO₂ have strong reducing capacity to remove pollutants, such as Cd(II), Hg(II), As(V), and Cr(VI), from water; these cations can be reduced into less toxic metallic or ion states. Dusadee et al. fabricated a titania-decorated reduced graphene oxide (TiO₂-rGO) nanocomposite via a hydrothermal process [110]. Studies on reducing the toxic Cr⁶⁺ (hexavalent chromium) ion toxicity using the titanium dioxide x/rGO numerical control have found that photocatalytic reduction of toxic Cr⁶⁺ generally increases with the increase in x. In addition, since rGO accelerates electron transport, the combination of photoexcited electrons and holes decreases leads to an increased duration of photocatalytic activity [118]. TiO₂ has facilitated many pollutant degradation processes such as the reduction of nitrate, the degradation of acid fuchsin, the decomposition of acetaldehyde, and the dechlorination of CCl₄ [119–122]. Due to the continued proliferation of environment pollutants, TiO₂ and other nanostructured materials should be vigorously developed in the future to improve the degradation of pollutants by photocatalysis.

6.1.2. Degradation of Air Pollutants

Just as industrial and technological developments can result in water pollution, so too can the atmosphere be adversely impacted by toxic pollutants that are emitted from chemical manufacturing plants, power plants, industrial facilities, transportation technologies, etc. Air pollution impacts the health of the global environment and the array of species that live within it, and new techniques are sought to reduce harmful airborne emissions. Highly efficient oxidation and reduction during

photocatalysis are considered to be an effective method to degrade inorganic and organic air pollutants to improve air quality [123–125]. Similarly, TiO₂ is considered the most promising photocatalyst. Kakeru et al. prepared TiO₂ nanoparticles with palladium sub-nanoclusters (<1 nm) using the flame aerosol technique [126]. Under sunlight, these materials can remove NO_x at approximately 3 to 7 times the rate of commercial TiO₂ (P25, Evonik) (without Pd). Natércia et al. prepared new composite materials of TiO₂ (P25) and N-doped carbon quantum dots (P25/NCQD) by a hydrothermal method, which was first used as the photooxidation catalyst of NO under the irradiation of ultraviolet and visible light [127]. The experiment showed that the conversion rate of the P25/NCQD composite material (27.0%) was more than twice that of P25 (10%) without modification, and the selectivity in visible light increased from 37.4% to 49.3%. The photocatalytic performance of the composite material in the UV region was also better than that of P25. Zeng et al. reported a H₂ reduction strategy to produce H-TiO₂ materials (with enhanced oxygen vacancy concentrations and distributions) that can promote formaldehyde decomposition in the dark [128]. Research of TiO₂-based photocatalysts has also been conducted to facilitate removal of tetrachloroethylene [129], acetone [130], benzene [131], phenol [73], etc. from the atmosphere.

6.2. Applications in Energy

6.2.1. Photocatalytic Hydrogen Generation

With the extensive use of nonrenewable fossil fuels, mankind is facing an unprecedented energy crisis. The photogenerated electrons on TiO₂ have strong reducing capacity, enabling hydrogen production from the photocatalytic splitting of water. Moreover, hydrogen combustion produces only water and no harmful emissions, and therefore its potential as a truly clean energy source has received considerable attention since it was discovered. Zou et al. reported a self-modified TiO₂ material with paramagnetic oxygen vacancies [132]. For the synthesis of V_o-TiO₂ (V_o: denotes a paramagnetic oxygen vacancy), they chose a porous amorphous TiO₂ material as a precursor that possessed a high surface area of 543 m² g⁻¹. The precursor was calcined in the presence of imidazole and hydrochloric acid at an elevated temperature in air to obtain the V_o-TiO₂ material [132]. The V_o-TiO₂ sample (for H₂ evolution from water) used methanol as a sacrificial reagent under visible light (≥400 nm) at room temperature, and the H₂ production rate was approximately 115 μmol h⁻¹ g⁻¹, which is substantially higher than that achieved with V_o-Ti³⁺-TiO₂ (32 μmol h⁻¹ g⁻¹). Zhou et al. introduced an ordered mesoporous black TiO₂ material that utilized a thermally stable and high surface area mesoporous TiO₂ as the hydrogenation precursor for treatment at 500 °C [133]. The samples possessed a relatively high surface area of 124 m² g⁻¹ and exhibited a photo response that extended from ultraviolet to visible light. As shown in Figure 22, the ordered mesoporous black TiO₂ material exhibits a high solar-driven hydrogen production rate (136.2 μmol h⁻¹), which is almost twice as high as that of pristine mesoporous TiO₂ (76.6 μmol h⁻¹). Zhong et al. constructed a covalently bonded oxidized graphitic C₃N₄/TiO₂ heterostructure that markedly increased the visible light photocatalytic activity for H₂ evolution by nearly a factor of approximately 6.1 compared to a simple physical mixture of TiO₂ nanosheets and O-g-C₃N₄ [134].

6.2.2. Photocatalytic CO₂ Reduction into Energy Fuels

In addition to reducing water to hydrogen, the photogenerated electrons on TiO₂ are capable of generating valuable solar energy fuels, such as CH₄, HCO₂H, CH₂O, CH₃OH, and CO₂, which are considered highly viable energy sources that can alleviate the problems associated with the production of greenhouse gases from the combustion of fossil fuels. Slamet et al. prepared Cu-doped TiO₂ through an improved impregnation method for photocatalytic CO₂ reduction [135]. Both the distribution of copper on the catalyst surface and the grain size of copper–titania catalysts (crystallite size of approximately 23 nm) were uniform, and it was determined that Cu doping can greatly enhance the photocatalytic performance of TiO₂ with respect to CO₂ reduction. Liu et al. found that

copper-loaded titania photocatalysts, prepared via a one-pot, sol-gel synthesis method, comprised highly dispersed copper and that CO₂ photoreduction exhibited a strong volcano dependence on Cu loading, which reflected the transition from 2-dimensional CuO_x nanostructures to 3-dimensional crystallites; optimum CH₄ production was observed for 0.03 wt.% Cu/TiO₂ [136].

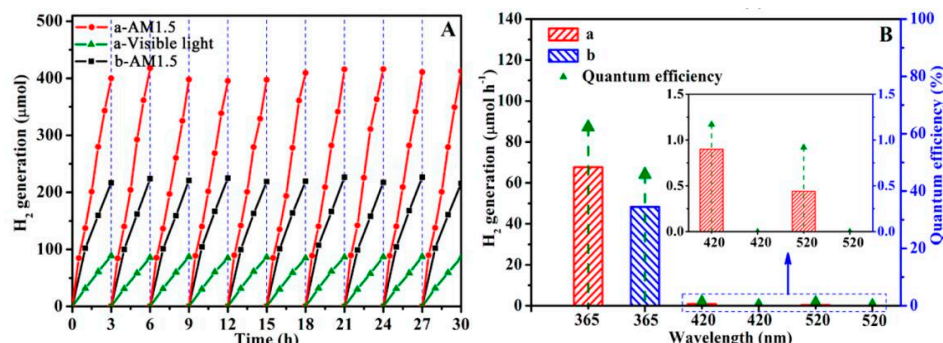


Figure 22. Photocatalytic hydrogen evolution of ordered mesoporous black TiO₂ (a) and pristine ordered mesoporous TiO₂ materials (b). (A) Cycling tests of photocatalytic hydrogen generation under AM 1.5 and visible light irradiation. (B) The photocatalytic hydrogen evolution rates under single-wavelength light and the corresponding QE. The inset enlarges the QE of single-wavelength light at 420 and 520 nm [133]. Copyright 2014 American Chemical Society.

6.2.3. Solar Batteries

Since semiconductors absorb photons to produce photonic carriers and the photonic carriers move and separate at the same time, electric energy can be obtained through charge transport. TiO₂ can also be applied to dye-sensitized solar cells, Li-ion batteries, Na-ion batteries, and supercapacitors. Liu et al. synthesized a spring-like Ti@TiO₂ nanowire array wire that could be used as a photoanode in dye-sensitized solar cells; this configuration exhibited a conversion efficiency maintenance rate of more than 95.95% [137]. Another study reported the use of anatase TiO₂ nanotubes on rutile TiO₂ nanorod arrays as photoanodes in quantum dot-sensitized solar cells, which have a small thickness of 1 μm and an excellent solar energy conversion efficiency of approximately 1.04%; this is almost 2.7 times higher than the conversion efficiencies measured for solar cells using the original TiO₂ nanorod array photoanodes, as shown in Figure 23 [138]. Chen et al. implemented a C@TiO₂ nanocomposite as the anode material for lithium-ion batteries, which utilize the esterification of ethylene glycol with acetic acid in the presence of potassium chloride. Li-ion batteries utilizing the C@TiO₂ nanocomposite anode exhibited excellent rate performance and specific capacity (237 mA h⁻¹ g⁻¹), and a coulomb efficiency (CE) of approximately 100% after 100 cycles [139]. Su et al. synthesized anatase TiO₂ via a template approach for use as the anode in Na-ion batteries; use of the template-synthesized TiO₂ resulted in better battery performance in comparison to that achieved when amorphous and rutile TiO₂ was used as the anode material. Compared to other crystalline phases of titanium dioxide, anatase titanium dioxide produced the highest capacity, 295 mA h⁻¹ g⁻¹, in the second cycle, tested at a current density of 20 mA g⁻¹ [140]. Kim et al. developed a black-colored TiO₂ nanotube array synthesized by electrochemical self-doping of an amorphous TiO₂ nanotube array and N₂ annealing; the material exhibited good stability, high capacitance, and electrocatalytic performance, and is an excellent material for supercapacitors and oxide anodes [141].

6.2.4. Supercapacitors

Yang et al. developed a hybrid material, covalently coupled ultrafine H-TiO₂ nanocrystals/nitrogen-doped graphene, via the hydrothermal route [142]. Due to the strong interaction between H-TiO₂ nanocrystals and NG plates, the high structural stability of the H-TiO₂ nanocrystal aggregation is inhibited. At the same time, the NG matrix plays the role of electron conductor and mechanical skeleton, imparting good stability and electrochemical activity on most of the well-dispersed ultrafine

H-TiO₂ nanocrystals [142]. The material exhibited a high reversible specific capacity of 385.2 F g⁻¹ at 1 A g⁻¹ and excellent cycling stability with 98.8% capacity retention. Parthiban et al. reported a blue titanium oxide (B-TiO₂) nanostructure that was applied via a one-pot hydrothermal route and hydrothermal oxidation [143]. The B-TiO₂ nanostructure indicated excellent cycling stability with approximately 90.2% capacitance retention after 10,000 charge–discharge cycles.

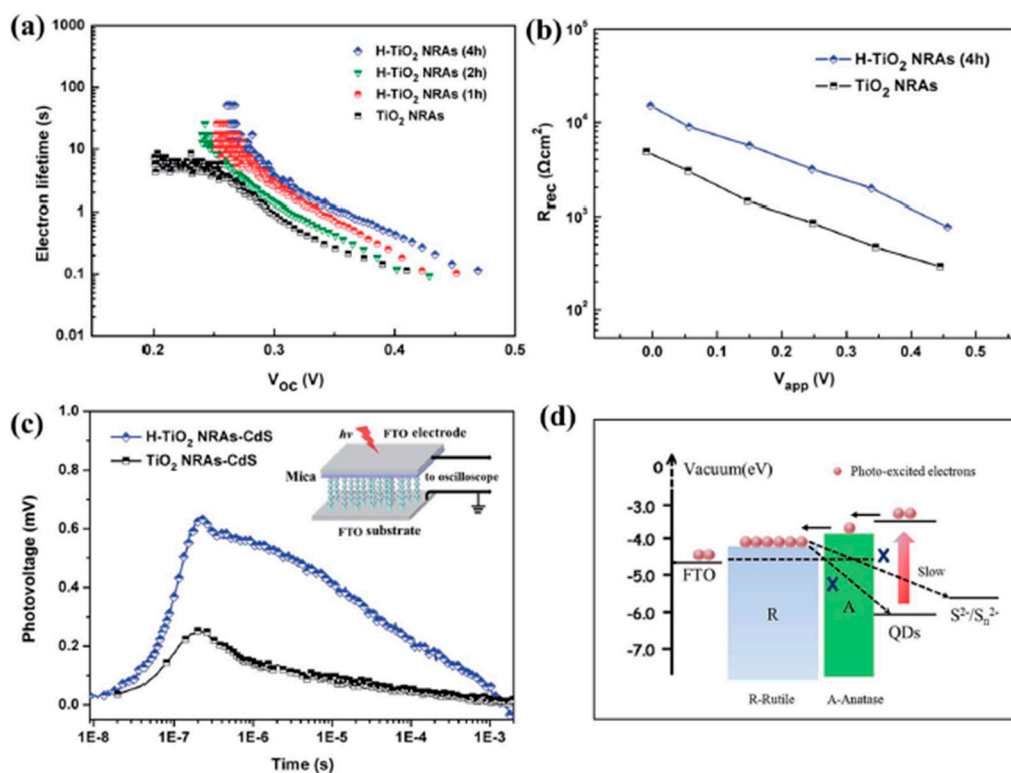


Figure 23. (a) Electron lifetime as a function of Voc for TiO₂ NRA and H-TiO₂ NRA electrodes with various reaction times. (b) Recombination resistance (R_{rec}) of the QDSCs made from TiO₂ NRAs and H-TiO₂ NRAs at various forward biases in the dark. (c) Transient photovoltage responses of CdS-TiO₂ NRAs and CdS-H-TiO₂ NRAs. The wavelength of the laser pulse was 532 nm. Inset: schematic setup of TPV measurements. (d) Schematic configuration for our device showing the interfacial charge transfer and recombination processes [138]. Copyright 2015 The Royal Society of Chemistry.

6.3. Other Applications

6.3.1. Antibacterial and Wound Healing

It is generally believed that electron–hole pairs formed under light illumination, such as •O²⁻ and •OH, not only destroy all chemical contaminants but also kill microorganisms. Liu et al. proposed a TiO₂/Ag₂O heterostructure (produced by a facile in situ precipitation route) to enhance antibacterial activities [144]. Yu et al. synthesized a TiO₂/BTO/Au heterostructured nanorod arrays (exhibiting piezophototronic and plasmonic effects) by using a simple process that combined hydrothermal and PVD methods. This material can be used as an antibacterial coating for efficient light driven in vitro/in vivo sterilization and wound healing [145].

6.3.2. Drug Delivery Carriers

TiO₂ has the advantages of nontoxicity, stability, biocompatibility, and natural abundance. The preparation of TiO₂ with a high specific surface area can be advantageous in drug delivery carrier applications. Johan et al. controlled the kinetics of drug delivery from mesoporous titania thin films via surface energy and pore size control [146]. Different pore sizes ranging from 3.4 nm

to 7.2 nm were achieved by the use of different structural guiding templates and expansive agents. In addition, by attaching dimethyl silane to the pore wall, the surface energy of the pore wall could be altered. The results indicated that the pore size and surface energy had significant effects on the adsorption and release kinetics of alendronate [146]. Biki et al. designed silica-supported mesoporous titania nanoparticles (MTN) coated with hyaluronic acid to cure breast cancer by effectively delivering doxorubicin (DOX) to the cancer cells [147]. Guo et al. deposited (onto the surface of MTN) hyaluronic acid and cyclic pentapeptide (ADH-1), which target CD44-overexpressing tumor cells and selectively inhibit the function of N-cadherin, respectively, to overcome the drug resistance of tumors [148].

Recently, Nakayama et al. found that H_2O_2 -treated TiO_2 can enhance the ability to produce reactive oxygen species (ROS) in response to X-ray irradiation [149]. As shown in Figure 24, the atomic packing factor (APF) intensity indicated that hydroxyl radical production in the TiO_x (H_2O_2 -treated TiO_2) nanoparticles increased in a radiation dose-dependent manner in comparison to that of the non- H_2O_2 -treated TiO_2 nanoparticles. This behavior allows H_2O_2 -treated TiO_2 nanoparticles to act as potential agents for enhancing the effects of radiation in the treatment of pancreatic cancer. Dai et al. designed and synthesized a novel nanodrug delivery system for the synergistic treatment of lung cancer [150]. They loaded DOX onto H_2O_2 -treated TiO_2 nanosheets. In this way, chemotherapy and radiotherapy were combined effectively for the synergistic therapy of cancers.

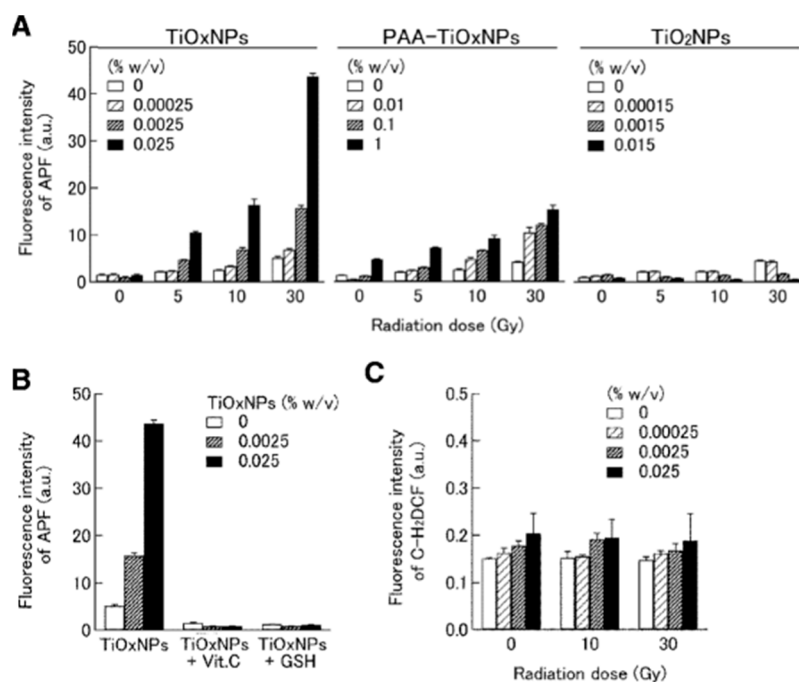


Figure 24. ROS production by the TiO_x NPs, PAA- TiO_x NPs, and TiO_2 NPs under X-ray irradiation. (A) Atomic packing factor (APF) intensity indicating that hydroxyl radical production in the TiO_x NPs and the PAA- TiO_x NPs increased in a radiation dose-dependent manner, but that of the TiO_2 NPs did not. Irradiated radiation doses were 0, 5, 10, and 30 Gy. Data are shown as the mean \pm SD from 5 independent experiments. (B) Production and scavenging of ROS by 1 mM vitamin C (Vit. C) or 1 mM glutathione (GSH). Histograms show the mean \pm SD calculated from 5 independent experiments. (C) Hydrogen peroxide production from the TiO_x NPs under X-ray irradiation [149]. Copyright 2016 Springer Nature Switzerland AG.

7. Conclusions

As discussed in this review article, TiO_2 -based nanomaterials with wide band gaps have advantages associated with natural geologic abundance, nontoxicity and stability but they also exhibit inherent deficiencies and limitations related to ineffective visible light responses and other

photocatalytic properties. The present review aimed to summarize key studies related to the marked enhancement of the photocatalytic performance of TiO₂ by analyzing its electrical structure and photocatalytic reaction process. We have highlighted TiO₂ photocatalysts with well-defined electrical and structure design, as well as tailored facets, dimensions, and remarkable morphologies, which are promising with respect to enhancing the photocatalytic properties of TiO₂. All works presented in this review has enabled the authors to obtain an in-depth understanding of the TiO₂ photocatalytic process, and the critical design of TiO₂ nanostructures with enhanced light absorption, high surface area, desired photostability, and charge carrier dynamics. We hope that this review will guide the future development of more robust TiO₂-based photocatalysts for large-scale applications.

Finally, photocatalysis technology is one of the most active research fields in the world in recent years. However, photocatalysis technologies based on TiO₂ semiconductor still suffer from several key scientific and technological problems, such as low solar energy utilization rate, inferior quantum yield, and difficult recovery, which greatly restricts its wide application in industry. The fundamental solution to improve solar energy absorption is energy band engineering, designing and regulating the bandgap to optimize the harvesting of incident photons. Narrow bandgap and direct semiconductor are more likely to make use of low energy light, but they are restricted by very high electron and hole recombination rate and the incompatible band-edge position. High quantum yield is inevitable for an idea photocatalysis in practical solar engineering, but it cannot be achieved simply doping or inducing intrinsic defects. More works are needed to do to search high quantum yield. All of the above problems depend on the deepening of basic research. Although at present, photocatalysis technology is still a long way from large-scale production and application, its huge potential excellent performance provides a good way for our development. In the near future, with the breakthrough of these key issues, the practical application of nano-photocatalytic materials will certainly be realized to improve our environment, provide cleaner energy, and bring more convenience to our daily life.

Author Contributions: X.K. and S.L. collected references, prepared figures, and wrote the original draft of the manuscript, they contributed equally to this work; Z.D. and Y.H. collected references and analyzed the data; X.S. gave valuable advice; Z.T. acted as a project director and contributed to subsequent revisions. All authors agreed to the final version of the paper.

Funding: This research was funded by the National Natural Science Foundation of China grant number 21571028, 21601027, the Fundamental Research Funds for the Central Universities grant number DUT16TD19, DUT17LK33, DUT18LK28 and the Education Department of the Liaoning Province of China grant number LT2015007.

Conflicts of Interest: The authors declare no conflicts of interest.

References

1. Fujishima, A.; Honda, K. Electrochemical photolysis of water at a semiconductor electrode. *Nature* **1972**, *238*, 37. [[CrossRef](#)] [[PubMed](#)]
2. Long, L.; Zhang, A.; Yang, J.; Zhang, X.; Yu, H. A green approach for preparing doped TiO₂ single crystals. *ACS Appl. Mater. Interfaces* **2014**, *6*, 16712–16720. [[CrossRef](#)]
3. Nakata, K.; Fujishima, A. TiO₂ photocatalysis: Design and applications. *J. Photochem. Photobio. C* **2012**, *13*, 169–189. [[CrossRef](#)]
4. Tong, H.; Ouyang, S.; Bi, Y.; Umezawa, N.; Oshikiri, M.; Ye, J. Nano-photocatalytic materials: Possibilities and challenges. *Adv. Mater.* **2012**, *24*, 229–251. [[CrossRef](#)]
5. Grätzel, M. Photoelectrochemical cells. *Nature* **2001**, *414*, 338. [[CrossRef](#)] [[PubMed](#)]
6. Ma, Y.; Wang, X.; Jia, Y.; Chen, X.; Han, H.; Li, C. Titanium dioxide-based nanomaterials for photocatalytic fuel generations. *Chem. Rev.* **2014**, *114*, 9987–10043. [[CrossRef](#)] [[PubMed](#)]
7. Schneider, J.; Matsuoka, M.; Takeuchi, M.; Zhang, J.; Horiuchi, Y.; Anpo, M.; Bahnemann, D.W. Understanding TiO₂ photocatalysis: Mechanisms and materials. *Chem. Rev.* **2014**, *114*, 9919–9986. [[CrossRef](#)]
8. Wang, M.; Iocozzia, J.; Sun, L.; Lin, C.; Lin, Z. Inorganic-modified semiconductor TiO₂ nanotube arrays for photocatalysis. *Energ. Environ. Sci.* **2014**, *7*, 2182–2202. [[CrossRef](#)]
9. Kalyanasundaram, K. Photochemical applications of solar energy: Photocatalysis and photodecomposition of water. *Photochemistry* **2013**, *41*, 182–265.

10. Liu, B.; Yang, J.; Zhao, X.; Yu, J. The role of electron interfacial transfer in mesoporous nano-TiO₂ photocatalysis: A combined study of in situ photoconductivity and numerical kinetic simulation. *Phys. Chem. Chem. Phys.* **2017**, *19*, 8866–8873. [[CrossRef](#)]
11. Liu, B.; Zhao, X.; Terashima, C.; Fujishima, A.; Nakata, K. Thermodynamic and kinetic analysis of heterogeneous photocatalysis for semiconductor systems. *Phys. Chem. Chem. Phys.* **2014**, *16*, 8751–8760. [[CrossRef](#)] [[PubMed](#)]
12. Ravelli, D.; Dondi, D.; Fagnoni, M.; Albini, A. Photocatalysis. A multi-faceted concept for green chemistry. *Chem. Soc. Rev.* **2009**, *38*, 1999–2011. [[CrossRef](#)] [[PubMed](#)]
13. Bai, S.; Jiang, J.; Zhang, Q.; Xiong, Y. Steering charge kinetics in photocatalysis: Intersection of materials syntheses, characterization techniques and theoretical simulations. *Chem. Soc. Rev.* **2015**, *44*, 2893–2939. [[CrossRef](#)] [[PubMed](#)]
14. Gao, M.; Zhu, L.; Ong, W.L.; Wang, J.; Ho, G.W. Structural design of TiO₂-based photocatalyst for H₂ production and degradation applications. *Catal. Sci. Technol.* **2015**, *5*, 4703–4726. [[CrossRef](#)]
15. Šuligoj, A.; Arčon, I.; Mazaj, M.; Dražič, G.; Arčon, D.; Cool, P.; Štangar, U.L.; Tušar, N.N. Surface modified titanium dioxide using transition metals: Nickel as a winning transition metal for solar light photocatalysis. *J. Mater. Chem. A* **2018**, *6*, 9882. [[CrossRef](#)]
16. Hou, Y.; Liu, S.; Zhang, J.; Cheng, X.; Wang, Y. Facile hydrothermal synthesis of TiO₂-Bi₂WO₆ hollow superstructures with excellent photocatalysis and recycle properties. *Dalton Trans.* **2014**, *43*, 1025–1031. [[CrossRef](#)] [[PubMed](#)]
17. Ansari, S.A.; Khan, M.M.; Ansari, M.O.; Cho, M.H. Nitrogen-doped titanium dioxide (N-doped TiO₂) for visible light photocatalysis. *New J. Chem.* **2016**, *40*, 3000–3009. [[CrossRef](#)]
18. Asahi, R.; Taga, Y.; Mannstadt, W.; Freeman, A.J. Electronic and optical properties of anatase TiO₂. *Phys. Rev. B* **2000**, *61*, 7459–7465. [[CrossRef](#)]
19. Park, H.; Choi, W. Effects of TiO₂ surface fluorination on photocatalytic reactions and photoelectrochemical behaviors. *J. Phys. Chem. B* **2004**, *108*, 4086–4093. [[CrossRef](#)]
20. Xu, J.; Ao, Y.; Fu, D.; Yuan, C. Low-temperature preparation of F-doped TiO₂ film and its photocatalytic activity under solar light. *Appl. Surf. Sci.* **2008**, *254*, 3033–3038. [[CrossRef](#)]
21. Niu, M.; Cui, R.; Wu, H.; Cheng, D.; Cao, D. Enhancement mechanism of the conversion efficiency of dye-sensitized solar cells based on nitrogen-, fluorine-, and iodine-doped TiO₂ photoanodes. *J. Phys. Chem. C* **2015**, *119*, 13425–13432. [[CrossRef](#)]
22. Liu, H.; Li, Y.; Yang, Y.; Mao, M.; Zeng, M.; Lan, L.; Yun, L.; Zhao, X. Highly efficient UV-Vis-infrared catalytic purification of benzene on CeMn_xO_y/TiO₂ nanocomposite, caused by its high thermocatalytic activity and strong absorption in the full solar spectrum region. *J. Mater. Chem. A* **2016**, *4*, 9890–9899. [[CrossRef](#)]
23. Narayan, H.; Alemu, H.; Macheli, L.; Thakurdesai, M.; Rao, T.K. Synthesis and characterization of Y³⁺-doped TiO₂ nanocomposites for photocatalytic applications. *Nanotechnology* **2009**, *20*, 255601. [[CrossRef](#)] [[PubMed](#)]
24. Wang, X.; Yuan, X.; Wang, D.; Dong, W.; Dong, C.; Zhang, Y.; Lin, T.; Huang, F. Tunable synthesis of colorful nitrogen-doped titanium oxide and its application in energy storage. *ACS Appl. Energy Mater.* **2018**, *1*, 876–882. [[CrossRef](#)]
25. Niu, P.; Wu, T.; Wen, L.; Tan, J.; Yang, Y.; Zheng, S.; Liang, Y.; Li, F.; Irvine, J.T.S.; Liu, G.; et al. Substitutional carbon-modified anatase TiO₂ decahedral plates directly derived from titanium oxalate crystals via topotactic transition. *Adv. Mater.* **2018**, *30*, e1705999. [[CrossRef](#)] [[PubMed](#)]
26. Zhao, X.; Liu, X.; Yu, M.; Wang, C.; Li, J. The highly efficient and stable Cu, Co, Zn-porphyrineTiO₂ photocatalysts with heterojunction by using fashioned one-step method. *Dyes Pigments* **2017**, *136*, 648–656. [[CrossRef](#)]
27. Hachiya, A.; Takata, S.; Komuro, Y.; Matsumoto, Y. Effects of V-ion doping on the photoelectrochemical properties of epitaxial TiO₂(110) thin films on Nb-doped TiO₂ (110) single crystals. *J. Phys. Chem. C* **2012**, *116*, 16951–16956. [[CrossRef](#)]
28. Klosek, S.; Raftery, D. Visible light driven V-doped TiO₂ photocatalyst and its photooxidation of ethanol. *J. Phys. Chem. B* **2001**, *105*, 2815–2819. [[CrossRef](#)]
29. Zahid, M.; Papadopoulou, E.L.; Suarato, G.; Binas, V.D.; Kiriakidis, G.; Gounaki, I.; Moira, O.; Venieri, D.; Bayer, I.S.; Athanassiou, A. Fabrication of visible light-induced antibacterial and self-cleaning cotton fabrics using manganese doped TiO₂ nanoparticles. *ACS Appl. Bio Mater.* **2018**, *1*, 1154–1164. [[CrossRef](#)]

30. Taguchi, T.; Ni, L.; Irie, H. Alkaline-resistant titanium dioxide thin film displaying visible-light-induced superhydrophilicity initiated by interfacial electron transfer. *Langmuir* **2013**, *29*, 4908–4914. [[CrossRef](#)]
31. Mizushima, K.; Tanaka, M.; Asai, A.; Iida, S.; Goodenough, B. Impurity levels of iron-group ions in TiO₂(II). *J. Phys. Chem. Solids* **1979**, *40*, 1129–1140. [[CrossRef](#)]
32. Borgarello, E.; Kiwi, J.; Grätzel, M.; Pelizzetti, E.; Viscald, M. Visible light induced water cleavage in colloidal solutions of chromium-doped titanium dioxide particles. *J. Am. Chem. Soc.* **1982**, *104*, 2996–3002. [[CrossRef](#)]
33. Xu, D.; Feng, L.; Lei, A. Characterizations of lanthanum trivalent ions/TiO₂ nanopowders catalysis prepared by plasma spray. *J. Colloid Interface Sci.* **2009**, *329*, 395–403. [[CrossRef](#)] [[PubMed](#)]
34. Li, N.; Zhou, X.; Liu, M.; Wei, L.; Shen, Q.; Bibi, R.; Xu, C.; Ma, Q.; Zhou, J. Enhanced visible light photocatalytic hydrogenation of CO₂ into methane over a Pd/Ce-TiO₂ nanocomposition. *J. Phys. Chem. C* **2017**, *121*, 25795–25804. [[CrossRef](#)]
35. Anandan, S.; Ikuma, Y.; Murugesan, V. Highly active rare-earth-metal La-doped photocatalysts: Fabrication, characterization, and their photocatalytic activity. *Int. J. Photoenergy* **2012**, *10*, 921412. [[CrossRef](#)]
36. Sun, L.; Zhao, X.; Cheng, X.; Sun, H.; Li, Y.; Li, P.; Fan, W. Synergistic effects in La/N codoped TiO₂ anatase (101) surface correlated with enhanced visible-light photocatalytic activity. *Langmuir* **2012**, *28*, 5882–5891. [[CrossRef](#)] [[PubMed](#)]
37. Choi, J.; Park, H.; Hoffman, M.R. Effects of single metal-ion doping on the visible-light photoreactivity of TiO₂. *J. Phys. Chem. C* **2010**, *114*, 783–792. [[CrossRef](#)]
38. Di Paola, A.; Ikeda, S.; Marci, G.; Ohtani, B.; Palmisano, L. Transition metal doped TiO₂: Physical properties and photocatalytic behaviour. *Int. J. Photoenergy* **2001**, *3*, 171. [[CrossRef](#)]
39. Asahi, R.; Morikawa, T.; Irie, H.; Ohwaki, T. Nitrogen-doped titanium dioxide as visible-light-sensitive photocatalyst: Designs, developments, and prospects. *Chem. Rev.* **2014**, *114*, 9824–9852. [[CrossRef](#)]
40. Muhich, C.L.; Westcott, J.Y.; Fuerst, T.; Weimer, A.W.; Musgrave, C.B. Increasing the photocatalytic activity of anatase TiO₂ through B, C, and N doping. *J. Phys. Chem. C* **2014**, *118*, 27415–27427. [[CrossRef](#)]
41. Asahi, R.; Morikawa, T.; Ohwaki, T.; Aoki, K.; Taga, Y. Visible-light photocatalysis in nitrogen-doped titanium oxides. *Science* **2001**, *13*, 269–271. [[CrossRef](#)]
42. Zhao, Z.; Fan, J.; Wang, J.; Li, R. Effect of heating temperature on photocatalytic reduction of CO₂ by N-TiO₂ nanotube catalyst. *Catal. Commun.* **2012**, *21*, 32–37. [[CrossRef](#)]
43. Irie, H.; Watanabe, Y.; Hashimoto, K. Nitrogen-concentration dependence on photocatalytic activity of TiO_{2-x}N_x powders. *J. Phys. Chem. B* **2003**, *107*, 5483–5486. [[CrossRef](#)]
44. Li, H.; Zhang, X.; Huo, Y.; Zhu, J. Supercritical preparation of a highly active S-doped TiO₂ photocatalyst for methylene blue mineralization. *Environ. Sci. Technol.* **2007**, *41*, 4410–4414. [[CrossRef](#)] [[PubMed](#)]
45. Liu, G.; Zhao, Y.; Sun, C.; Li, F.; Lu, G.Q.; Cheng, H.M. Synergistic effects of B/N doping on the visible-light photocatalytic activity of mesoporous TiO₂. *Angew. Chem. Int. Ed.* **2008**, *47*, 4516–4520. [[CrossRef](#)] [[PubMed](#)]
46. Peighambaroust, N.S.; Asl, S.K.; Mohammadpour, R.; Asl, S.K. Band-gap narrowing and electrochemical properties in N-doped and reduced anodic TiO₂ nanotube arrays. *Electrochim. Acta* **2018**, *270*, 245–255. [[CrossRef](#)]
47. Lynch, J.; Giannini, C.; Cooper, J.K.; Loiudice, A.; Sharp, I.D.; Buonsanti, R. Substitutional or interstitial site-selective nitrogen doping in TiO₂ nanostructures. *J. Phys. Chem. C* **2015**, *119*, 7443–7452. [[CrossRef](#)]
48. Di Valentin, C.; Finazzi, E.; Pacchioni, G.; Selloni, A.; Livraghi, S.; Paganini, M.C.; Giamello, E. N-doped TiO₂: Theory and experiment. *Chem. Phys.* **2007**, *339*, 44–56. [[CrossRef](#)]
49. Wu, Y.; Lazic, P.; Hautier, G.; Persson, K.; Ceder, G. First principles high throughput screening of oxynitrides for water-splitting photocatalysts. *Energy Environ. Sci.* **2013**, *6*, 157–168. [[CrossRef](#)]
50. Wang, J.; Tafen, D.N.; Lewis, J.P.; Hong, Z.; Manivannan, A.; Zhi, M.; Li, M.; Wu, N. Origin of photocatalytic activity of nitrogen-doped TiO₂ nanobelts. *J. Am. Chem. Soc.* **2009**, *131*, 12290–12297. [[CrossRef](#)]
51. Zhang, P.; Tachikawa, T.; Fujitsuka, M.; Majima, T. In situ fluorine doping of TiO₂ superstructures for efficient visible-light driven hydrogen generation. *ChemSusChem* **2016**, *9*, 617–623. [[CrossRef](#)] [[PubMed](#)]
52. Seo, H.; Baker, L.R.; Hervier, A.; Kim, J.; Whitten, J.L.; Somorjai, G.A. Generation of highly n-type titanium oxide using plasma fluorine insertion. *Nano Lett.* **2011**, *11*, 751–756. [[CrossRef](#)] [[PubMed](#)]
53. Yu, W.; Liu, X.; Pana, L.; Li, J.; Liu, J.; Zhang, J.; Li, P.; Chen, C.; Sun, Z. Enhanced visible light photocatalytic degradation of methylene blue by F-doped TiO₂. *Appl. Surf. Sci.* **2014**, *319*, 107–112. [[CrossRef](#)]
54. Chen, X.; Liu, L.; Yu, P.Y.; Mao, S.S. Increasing solar absorption for photocatalysis with black hydrogenated titanium dioxide nanocrystals. *Science* **2011**, *331*, 746–749. [[CrossRef](#)] [[PubMed](#)]

55. Song, H.; Li, C.; Lou, Z.; Ye, Z.; Zhu, L. Effective formation of oxygen vacancies in black TiO₂ nanostructures with efficient solar-driven water splitting. *ACS Sustain. Chem. Eng.* **2017**, *5*, 8982–8987. [[CrossRef](#)]
56. Hu, Y.H. A highly efficient photocatalyst–hydrogenated black TiO₂ for the photocatalytic splitting of water. *Angew. Chem. Int. Ed.* **2012**, *51*, 12410–12412. [[CrossRef](#)] [[PubMed](#)]
57. Lin, L.; Huang, J.; Li, X.; Abass, M.A.; Zhang, S. Effective surface disorder engineering of metal oxide nanocrystals for improved photocatalysis. *Appl. Catal. B Environ.* **2017**, *203*, 615–624. [[CrossRef](#)]
58. Liu, N.; Haublein, V.; Zhou, X.; Venkatesan, U.; Hartmann, M.; Mackovic, M.; Nakajima, T.; Spiecker, E.; Osvet, A.; Frey, L.; Schmuki, P. “Black” TiO₂ nanotubes formed by high-energy proton implantation show noble-metal-co-catalyst free photocatalytic H₂-evolution. *Nano Lett.* **2015**, *15*, 6815–6820. [[CrossRef](#)]
59. Wang, G.; Wang, H.; Ling, Y.; Tang, Y.; Yang, X.; Fitzmorris, R.C.; Wang, C.; Zhang, J.Z.; Li, Y. Hydrogen-treated TiO₂ nanowire arrays for photoelectrochemical water splitting. *Nano Lett.* **2011**, *11*, 3026–3033. [[CrossRef](#)]
60. Wang, X.; Fu, R.; Yin, Q.; Wu, H.; Guo, X.; Xu, R.; Zhong, Q. Black TiO₂ synthesized via magnesiothermic reduction for enhanced photocatalytic activity. *J. Nanopart. Res.* **2018**, *20*, 89. [[CrossRef](#)]
61. Dong, J.; Han, J.; Liu, Y.; Nakajima, A.; Matsushita, S.; Wei, S.; Gao, W. Defective black TiO₂ synthesized via anodization for visible-light photocatalysis. *ACS Appl. Mater. Interfaces* **2014**, *6*, 1385–1388. [[CrossRef](#)] [[PubMed](#)]
62. Liu, X.; Gao, S.; Xu, H.; Lou, Z.; Wang, W.; Huang, B.; Dai, Y. Green synthetic approach for Ti³⁺ self-doped TiO_{2-x} nanoparticles with efficient visible light photocatalytic activity. *Nanoscale* **2013**, *5*, 1870–1875. [[CrossRef](#)] [[PubMed](#)]
63. Chen, S.; Wang, Y.; Li, J.; Hu, Z.; Zhao, H.; Xie, W.; Wei, Z. Synthesis of black TiO₂ with efficient visible-light photocatalytic activity by ultraviolet light irradiation and low temperature annealing. *Mater. Res. Bull.* **2018**, *98*, 280–287. [[CrossRef](#)]
64. Liu, L.; Yu, P.Y.; Chen, X.; Mao, S.S.; Shen, D.Z. Hydrogenation and disorder in engineered black TiO₂. *Phys. Rev. Lett.* **2013**, *111*, 065505. [[CrossRef](#)] [[PubMed](#)]
65. Fujishima, A.; Zhang, X.; Tryk, D.A. TiO₂ photocatalysis and related surface phenomena. *Surf. Sci. Rep.* **2008**, *63*, 515–582. [[CrossRef](#)]
66. Pan, X.; Yang, M.Q.; Fu, X.; Zhang, N.; Xu, Y.J. Defective TiO₂ with oxygen vacancies: Synthesis, properties and photocatalytic applications. *Nanoscale* **2013**, *5*, 3601–3614. [[CrossRef](#)] [[PubMed](#)]
67. Tan, H.; Zhao, Z.; Niu, M.; Mao, C.; Cao, D.; Cheng, D.; Feng, P.; Sun, Z. A facile and versatile method for preparation of colored TiO₂ with enhanced solar-driven photocatalytic activity. *Nanoscale* **2014**, *6*, 10216–10223. [[CrossRef](#)]
68. Li, S.; Qiu, J.; Ling, M.; Peng, F.; Wood, B.; Zhang, S. Photoelectrochemical characterization of hydrogenated TiO₂ nanotubes as photoanodes for sensing applications. *ACS Appl. Mater. Interfaces* **2013**, *5*, 11129–11135. [[CrossRef](#)]
69. Wang, Z.; Yang, C.; Lin, T.; Yin, H.; Chen, P.; Wan, D.; Xu, F.; Huang, F.; Lin, J.; Xie, X.; Jiang, M. H-doped black titania with very high solar absorption and excellent photocatalysis enhanced by localized surface plasmon resonance. *Adv. Funct. Mater.* **2013**, *23*, 5444–5450. [[CrossRef](#)]
70. Sinhamahapatra, A.; Jeon, J.-P.; Yu, J.-S. A new approach to prepare highly active and stable black titania for visible light-assisted hydrogen production. *Energ. Environ. Sci.* **2015**, *8*, 3539–3544. [[CrossRef](#)]
71. Zhou, L.; Boyle, D.S.; O’Brien, P. A facile synthesis of uniform NH₄TiOF₃ mesocrystals and their conversion to TiO₂ mesocrystals. *J. Am. Chem. Soc.* **2008**, *130*, 1309–1320. [[CrossRef](#)]
72. Kang, X.; Han, Y.; Song, X.; Tan, Z. A facile photoassisted route to synthesis N, F-codoped oxygen-deficient TiO₂ with enhanced photocatalytic performance under visible light irradiation. *Appl. Surf. Sci.* **2018**, *434*, 725–734. [[CrossRef](#)]
73. Kang, X.; Song, X.-Z.; Han, Y.; Cao, J.; Tan, Z. Defect-engineered TiO₂ hollow spiny nanocubes for phenol degradation under visible light irradiation. *Sci. Rep.* **2018**, *8*, 5904. [[CrossRef](#)]
74. Li, X.; Yu, J.; Jaroniec, M. Hierarchical photocatalysts. *Chem. Soc. Rev.* **2016**, *45*, 2603–2636. [[CrossRef](#)] [[PubMed](#)]
75. Yang, H.G.; Zeng, H.C. Preparation of hollow anatase TiO₂ nanospheres via Ostwald ripening. *J. Phys. Chem. B* **2004**, *108*, 3492–3495. [[CrossRef](#)]

76. Pan, J.H.; Zhang, X.; Du, A.J.; Sun, D.D.; Leckie, J.O. Self-etching reconstruction of hierarchically mesoporous F-TiO₂ hollow microspherical photocatalyst for concurrent membrane water purifications. *J. Am. Chem. Soc.* **2008**, *130*, 11256–11257. [[CrossRef](#)] [[PubMed](#)]
77. Cao, J.; Song, X.-Z.; Kang, X.; Dai, Z.; Tan, Z. One-pot synthesis of oleic acid modified monodispersed mesoporous TiO₂ nanospheres with enhanced visible light photocatalytic performance. *Adv. Powder Technol.* **2018**, *29*, 1925–1932. [[CrossRef](#)]
78. Banerjee, A.N. The design, fabrication, and photocatalytic utility of nanostructured semiconductors: Focus on TiO₂-based nanostructures. *Nanotechnol. Sci. Appl.* **2011**, *4*, 35–65. [[CrossRef](#)]
79. Lee, S.-Y.; Park, S.-J. TiO₂ photocatalyst for water treatment applications. *J. Ind. Eng. Chem.* **2013**, *19*, 1761–1769. [[CrossRef](#)]
80. Pauzauskie, P.J.; Yang, P. Nanowire photonics. *Mater. Today* **2006**, *9*, 36–45. [[CrossRef](#)]
81. Yan, R.; Gargas, D.; Yang, P. Nanowire photonics. *Nature Photonics* **2009**, *3*, 569. [[CrossRef](#)]
82. Zhou, X.; Liu, N.; Schmuki, P. Photocatalysis with TiO₂ nanotubes: “Colorful” reactivity and designing site-specific photocatalytic centers into TiO₂ nanotubes. *ACS Catal.* **2017**, *7*, 3210–3235. [[CrossRef](#)]
83. Shibata, T.; Sakai, N.; Fukuda, K.; Ebina, Y.; Sasaki, T. Photocatalytic properties of titania nanostructured films fabricated from Titania nanosheets. *Phys. Chem. Chem. Phys.* **2007**, *9*, 2413–2420. [[CrossRef](#)] [[PubMed](#)]
84. Shichi, T.; Katsumata, K.-I. Development of photocatalytic self-cleaning glasses utilizing metal oxide nanosheets. *J. Surf. Finish. Soc. Jpn* **2010**, *61*, 30–35. [[CrossRef](#)]
85. Ong, W.-J.; Tan, L.-L.; Chai, S.-P.; Yong, S.-T.; Mohamed, A.R. Highly reactive {001} facets of TiO₂-based composites: Synthesis, formation mechanism and characterization. *Nanoscale* **2014**, *6*, 1946–2008. [[CrossRef](#)] [[PubMed](#)]
86. Sun, L.; Zhao, Z.; Zhou, Y.; Liu, L. Anatase TiO₂ nanocrystals with exposed {001} facets on graphene sheets via molecular grafting for enhanced photocatalytic activity. *Nanoscale* **2012**, *4*, 613–620. [[CrossRef](#)] [[PubMed](#)]
87. Yang, H.G.; Sun, C.H.; Qiao, S.Z.; Zou, J.; Liu, G.; Smith, S.C.; Cheng, H.M.; Lu, G.Q. Anatase TiO₂ single crystals with a large percentage of reactive facets. *Nature* **2008**, *453*, 638–641. [[CrossRef](#)]
88. Tan, Z.; Sato, K.; Takami, S.; Numako, C.; Umetsu, M.; Soga, K.; Nakayama, M.; Sasaki, R.; Tanaka, T.; Ogino, C.; et al. Particle size for photocatalytic activity of anatase TiO₂ nanosheets with highly exposed {001} facets. *RSC Adv.* **2013**, *3*, 19268–19271. [[CrossRef](#)]
89. Liu, G.; Yang, H.G.; Pan, J.; Yang, Y.Q.; Lu, G.Q.; Cheng, H.M. Titanium dioxide crystals with tailored facets. *Chem. Rev.* **2014**, *114*, 9559–9612. [[CrossRef](#)]
90. Zheng, Z.; Huang, B.; Qin, X.; Zhang, X.; Dai, Y.; Jiang, M.; Wang, P.; Whangbo, M.H. Highly efficient photocatalyst: TiO₂ microspheres produced from TiO₂ nanosheets with a high percentage of reactive {001} facets. *Chemistry* **2009**, *15*, 12576–12579. [[CrossRef](#)]
91. Wang, J.; Zhang, P.; Li, X.; Zhu, J.; Li, H. Synchronical pollutant degradation and H₂ production on a Ti³⁺-doped TiO₂ visible photocatalyst with dominant (001) facets. *Appl. Catal. B Environ.* **2013**, *134–135*, 198–204. [[CrossRef](#)]
92. Banerjee, B.; Amoli, V.; Maurya, A.; Sinha, A.K.; Bhaumik, A. Green synthesis of Pt-doped TiO₂ nanocrystals with exposed (001) facets and mesoscopic void space for photo-splitting of water under solar irradiation. *Nanoscale* **2015**, *7*, 10504–10512. [[CrossRef](#)] [[PubMed](#)]
93. Fattakhova-Rohlfing, D.; Zaleska, A.; Bein, T. Three-dimensional titanium dioxide nanomaterials. *Chem. Rev.* **2014**, *114*, 9487–9558. [[CrossRef](#)] [[PubMed](#)]
94. Xiong, T.; Dong, F.; Wu, Z. Enhanced extrinsic absorption promotes the visible light photocatalytic activity of wide band-gap (BiO)₂CO₃ hierarchical structure. *RSC Adv.* **2014**, *4*, 56307–56312. [[CrossRef](#)]
95. Li, H.; Bian, Z.; Zhu, J.; Zhang, D.; Li, G.; Huo, Y.; Li, H.; Lu, Y. Mesoporous titania spheres with tunable chamber structure and enhanced photocatalytic activity. *J. Am. Chem. Soc.* **2007**, *129*, 8406–8407. [[CrossRef](#)] [[PubMed](#)]
96. Kondo, Y.; Yoshikawa, H.; Awaga, K.; Murayama, M.; Mori, T.; Sunada, K.; Bandow, S.; Iijima, S. Preparation, photocatalytic activities, and dye-sensitized solar-cell performance of submicron-scale TiO₂ hollow spheres. *Langmuir* **2008**, *24*, 547–550. [[CrossRef](#)] [[PubMed](#)]
97. Wang, L.; Takayoshi, S.; Ebina, Y.; Kurashima, K.; Watanabe, M. Fabrication of controllable ultrathin hollow shells by layer-by-layer assembly of exfoliated titania nanosheets on polymer templates. *Chem. Mater.* **2002**, *14*, 4827–4832. [[CrossRef](#)]

98. Zhao, T.; Liu, Z.; Nakata, K.; Nishimoto, S.; Murakami, T.; Zhao, Y.; Jiang, L.; Fujishima, A. Multichannel TiO₂ hollow fibers with enhanced photocatalytic activity. *J. Mater. Chem.* **2010**, *20*, 5095–5099. [[CrossRef](#)]
99. Shang, S.; Jiao, X.; Chen, D. Template-free fabrication of TiO₂ hollow spheres and their photocatalytic properties. *ACS Appl. Mater. Interfaces* **2012**, *4*, 860–865. [[CrossRef](#)]
100. Song, R.Q.; Colfen, H. Mesocrystals-ordered nanoparticle superstructures. *Adv. Mater.* **2010**, *22*, 1301–1330. [[CrossRef](#)]
101. Colfen, H.; Antonietti, M. Mesocrystals: Inorganic superstructures made by highly parallel crystallization and controlled alignment. *Angew. Chem. Int. Ed.* **2005**, *44*, 5576–5591. [[CrossRef](#)] [[PubMed](#)]
102. Cai, J.; Qi, L. TiO₂ mesocrystals: Synthesis, formation mechanisms and applications. *Sci. China Chem.* **2012**, *55*, 2318–2326. [[CrossRef](#)]
103. Zhang, P.; Tachikawa, T.; Bian, Z.; Majima, T. Selective photoredox activity on specific facet-dominated TiO₂ mesocrystal superstructures incubated with directed nanocrystals. *Appl. Catal. B Environ.* **2015**, *176–177*, 678–686. [[CrossRef](#)]
104. Zhang, P.; Tachikawa, T.; Fujitsuka, M.; Majima, T. Efficient charge separation on 3D architectures of TiO₂ mesocrystals packed with a chemically exfoliated MoS₂ shell in synergetic hydrogen evolution. *Chem. Commun.* **2015**, *51*, 7187–7190. [[CrossRef](#)] [[PubMed](#)]
105. Zhang, P.; Fujitsuka, M.; Majima, T. TiO₂ mesocrystal with nitrogen and fluorine codoping during topochemical transformation: Efficient visible light induced photocatalyst with the codopants. *Appl. Catal. B Environmental* **2016**, *185*, 181–188. [[CrossRef](#)]
106. Elbanna, O.; Fujitsuka, M.; Majima, T. g-C₃N₄/TiO₂ Mesocrystals composite for H₂ evolution under visible-light irradiation and its charge carrier dynamics. *ACS Appl. Mater. Interfaces* **2017**, *9*, 34844–34854. [[CrossRef](#)] [[PubMed](#)]
107. Ossama Elbanna, S.K. Mamoru Fujitsuka and Tetsuro Majima, TiO₂ mesocrystals composited with gold nanorods for highly efficient visible-NIR-photocatalytic hydrogen production. *Nano Energy* **2017**, *17*, 1842.
108. Kang, X.; Song, X.-Z.; Liu, S.; Pei, M.; Wen, W.; Tan, Z. In situ formation of defect-engineered N-doped TiO₂ porous mesocrystal for enhanced photo-degradation and PEC performance. *Nanoscale Adv.* **2019**. [[CrossRef](#)]
109. Choi, Y.; Ko, M.S.; Bokare, A.D.; Kim, D.-H.; Bahnemann, D.W.; Choi, W. Sequential process combination of photocatalytic oxidation and dark reduction for the removal of organic pollutants and Cr(VI) using Ag/TiO₂. *Environ. Sci. Technol.* **2017**, *51*, 3975–3981. [[CrossRef](#)]
110. Kim, S.; Park, H. Sunlight-harnessing and storing heterojunction TiO₂/Al₂O₃/WO₃ electrodes for night-time applications. *RSC Adv.* **2013**, *3*, 17551–17558. [[CrossRef](#)]
111. Tatsuma, T.; Saitoh, S.; Ohko, Y.; Fujishima, A. TiO₂-WO₃ photoelectrochemical anticorrosion system with an energy storage ability. *Chem. Mater.* **2001**, *13*, 2838–2842. [[CrossRef](#)]
112. Li, J.; Cushing, S.K.; Zheng, P.; Senty, T.; Meng, F.; Bristow, A.D.; Manivannan, A.; Wu, N. Solar hydrogen generation by a CdS-Au-TiO₂ sandwich nanorod array enhanced with Au nanoparticle as electron relay and plasmonic photosensitizer. *J. Am. Chem. Soc.* **2014**, *136*, 8438–8449. [[CrossRef](#)] [[PubMed](#)]
113. Hu, L.; Zhang, Y.; Zhang, S.; Li, B. A transparent TiO₂-C@TiO₂-graphene free-standing film with enhanced visible light photocatalysis. *RSC Adv.* **2016**, *6*, 43098–43103. [[CrossRef](#)]
114. Wang, W.; Ni, Y.; Lu, C.; Xu, Z. Hydrogenation of TiO₂ nanosheets with exposed {001} facets for enhanced photocatalytic activity. *RSC Adv.* **2012**, *2*, 8286–8288.
115. Plodinec, M.; Grcic, I.; Willinger, M.G.; Hammud, A.; Huang, X.; Panzic, I.; Gajovic, A. Black TiO₂ nanotube arrays decorated with Ag nanoparticles for enhanced visible-light photocatalytic oxidation of salicylic acid. *J. Alloys Comp.* **2019**, *776*, 883–896. [[CrossRef](#)]
116. Ling, H.; Kim, K.; Liu, Z.; Shi, J.; Zhu, X.; Huang, J. Photocatalytic degradation of phenol in water on as-prepared and surface modified TiO₂ nanoparticles. *Catal. Today* **2015**, *258*, 96–102. [[CrossRef](#)]
117. Hao, X.; Li, M.; Zhang, L.; Wang, K.; Liu, C. Photocatalyst TiO₂/WO₃/GO nano-composite with high efficient photocatalytic performance for BPA degradation under visible light and solar light illumination. *J. Ind. Eng. Chem.* **2017**, *55*, 140–148. [[CrossRef](#)]
118. Khamboonrueang, D.; Srirattanapibul, S.; Tang, I.-M.; Thongmee, S. TiO₂-rGO nanocomposite as a photo catalyst for the reduction of Cr⁶⁺. *Mater. Res. Bull.* **2018**, *107*, 236–241. [[CrossRef](#)]
119. Ren, H.-T.; Jia, S.-Y.; Zou, J.-J.; Wu, S.-H.; Han, X. A facile preparation of Ag₂O/P25 photocatalyst for selective reduction of nitrate. *Appl. Catal. B Environ.* **2015**, *176–177*, 53–61. [[CrossRef](#)]

120. Fan, C.; Chen, C.; Wang, J.; Fu, X.; Ren, Z.; Qian, G.; Wang, Z. Black hydroxylated titanium dioxide prepared via ultrasonication with enhanced photocatalytic activity. *Sci. Rep.* **2015**, *5*, 11712. [[CrossRef](#)]
121. Vequizo, J.J.M.; Matsunaga, H.; Ishiku, T.; Kamimura, S.; Ohno, T.; Yamakata, A. Trapping-induced enhancement of photocatalytic activity on brookite TiO₂ powders: Comparison with anatase and rutile TiO₂ powders. *ACS Catal.* **2017**, *7*, 2644–2651. [[CrossRef](#)]
122. Kim, S.; Moon, G.-h.; Kim, G.; Kang, U.; Park, H.; Choi, W. TiO₂ complexed with dopamine-derived polymers and the visible light photocatalytic activities for water pollutants. *J. Catal.* **2017**, *346*, 92–100. [[CrossRef](#)]
123. Huang, H.L.; Lee, W.G.; Wu, F.S. Emissions of air pollutants from indoor charcoal barbecue. *J. Hazard. Mater.* **2016**, *302*, 198–207. [[CrossRef](#)] [[PubMed](#)]
124. Rodrigues, S.; Ranjit, K.T.; Uma, S.; Martyanov, I.N.; Klabunde, K.J. Single-step synthesis of a highly active visible-light photocatalyst for oxidation of a common indoor air pollutant: Acetaldehyde. *Adv. Mater.* **2005**, *17*, 2467–2471. [[CrossRef](#)]
125. Lyu, J.; Zhu, L.; Burda, C. Considerations to improve adsorption and photocatalysis of low concentration air pollutants on TiO₂. *Catal. Today* **2014**, *225*, 24–33. [[CrossRef](#)]
126. Fujiwara, K.; Müller, U.; Pratsinis, S.E. Pd subnano-clusters on TiO₂ for solar-light removal of NO. *ACS Catal.* **2016**, *6*, 1887–1893. [[CrossRef](#)]
127. Martins, N.C.T.; Ângelo, J.; Girão, A.V.; Trindade, T.; Andrade, L.; Mendes, A. N-doped carbon quantum dots/TiO₂ composite with improved photocatalytic activity. *Appl. Catal. B Environ.* **2016**, *193*, 67–74. [[CrossRef](#)]
128. Zeng, L.; Song, W.; Li, M.; Zeng, D.; Xie, C. Catalytic oxidation of formaldehyde on surface of H-TiO₂/H-C-TiO₂ without light illumination at room temperature. *Appl. Catal. B Environ.* **2014**, *147*, 490–498. [[CrossRef](#)]
129. Yamazaki, S.; Tsukamoto, H.; Araki, K.; Tanimura, T.; Tejedor-Tejedor, I.; Anderson, M.A. Photocatalytic degradation of gaseous tetrachloroethylene on porous TiO₂ pellets. *Appl. Catal. B Environ.* **2001**, *33*, 109–117. [[CrossRef](#)]
130. Hernández-Alonso, M.D.; Tejedor-Tejedor, I.; Coronado, J.M.; Anderson, M.A.; Soria, J. Operando FTIR study of the photocatalytic oxidation of acetone in air over TiO₂-ZrO₂ thin film. *Catal. Today* **2009**, *143*, 364–373. [[CrossRef](#)]
131. Xu, Y.-J.; Zhuang, Y.; Fu, X. New insight for enhanced photocatalytic Activity of TiO₂ by doping carbon nanotubes: A case study on degradation of benzene and methyl orange. *J. Phys. Chem. C.* **2010**, *114*, 2669–2676. [[CrossRef](#)]
132. Zou, X.; Liu, J.; Su, J.; Zuo, F.; Chen, J.; Feng, P. Facile synthesis of thermal- and photostable titania with paramagnetic oxygen vacancies for visible-light photocatalysis. *Chemistry* **2013**, *1*, 2866–2873. [[CrossRef](#)]
133. Zhou, W.; Li, W.; Wang, J.Q.; Qu, Y.; Yang, Y.; Xie, Y.; Zhang, K.; Wang, L.; Fu, H.; Zhao, D. Ordered mesoporous black TiO(2) as highly efficient hydrogen evolution photocatalyst. *J. Am. Chem. Soc.* **2014**, *136*, 9280–9283. [[CrossRef](#)] [[PubMed](#)]
134. Zhong, R.; Zhang, Z.; Yi, H.; Zeng, L.; Tang, C.; Huang, L.; Gu, M. Covalently bonded 2D/2D O-g-C₃N₄/TiO₂ heterojunction for enhanced visible-light photocatalytic hydrogen evolution. *Appl. Catal. B Environ.* **2018**, *237*, 1130–1138. [[CrossRef](#)]
135. Slamet; Nasution, H.W.; Purnama, E.; Kosela, S.; Gunlazuardi, J. Photocatalytic reduction of CO₂ on copper-doped Titania catalysts prepared by improved-impregnation method. *Catal. Commun.* **2005**, *6*, 313–319. [[CrossRef](#)]
136. Liu, D.; Fernández, Y.; Ola, O.; Mackintosh, S.; Maroto-Valer, M.; Parlett, C.M.A.; Lee, A.F.; Wu, J.C.S. On the impact of Cu dispersion on CO₂ photoreduction over Cu/TiO₂. *Catal. Commun.* **2012**, *25*, 78–82. [[CrossRef](#)]
137. Liu, G.; Wang, H.; Wang, M.; Liu, W.; Ardhi, R.E.A.; Zou, D.; Lee, J.K. Study on a stretchable, fiber-shaped, and TiO₂ nanowire array-based dye-sensitized solar cell with electrochemical impedance spectroscopy method. *Electrochim. Acta* **2018**, *267*, 34–40. [[CrossRef](#)]
138. Liu, B.; Sun, Y.; Wang, X.; Zhang, L.; Wang, D.; Fu, Z.; Lin, Y.; Xie, T. Branched hierarchical photoanode of anatase TiO₂ nanotubes on rutile TiO₂ nanorod arrays for efficient quantum dot-sensitized solar cells. *J. Mater. Chem. A* **2015**, *3*, 4445–4452. [[CrossRef](#)]
139. Chen, J.; Li, Y.; Mu, J.; Zhang, Y.; Yu, Z.; Han, K.; Zhang, L. C@TiO₂ nanocomposites with impressive electrochemical performances as anode material for lithium-ion batteries. *J. Alloys Comp.* **2018**, *742*, 828–834. [[CrossRef](#)]

140. Su, D.; Dou, S.; Wang, G. Anatase TiO₂: Better anode material than amorphous and rutile phases of TiO₂ for Na-ion batteries. *Chem. Mater.* **2015**, *27*, 6022–6029. [[CrossRef](#)]
141. Kim, C.; Kim, S.; Lee, J.; Kim, J.; Yoon, J. Capacitive and oxidant generating properties of black-colored TiO₂ nanotube array fabricated by electrochemical self-doping. *ACS Appl. Mater. Interfaces* **2015**, *7*, 7486–7491. [[CrossRef](#)] [[PubMed](#)]
142. Yang, S.; Lin, Y.; Song, X.; Zhang, P.; Gao, L. Covalently coupled ultrafine H-TiO₂ nanocrystals/nitrogen-doped graphene hybrid materials for high-performance supercapacitor. *ACS Appl. Mater. Interfaces* **2015**, *7*, 17884–17892. [[CrossRef](#)] [[PubMed](#)]
143. Pazhamalai, P.; Krishnamoorthy, K.; Mariappan, V.K.; Kim, S.J. Blue TiO₂ nanosheets as a high-performance electrode material for supercapacitors. *J. Colloid Interface Sci.* **2019**, *536*, 62–70. [[CrossRef](#)] [[PubMed](#)]
144. Liu, B.; Mu, L.; Han, B.; Zhang, J.; Shi, H. Fabrication of TiO₂/Ag₂O heterostructure with enhanced photocatalytic and antibacterial activities under visible light irradiation. *Appl. Surf. Sci.* **2017**, *396*, 1596–1603. [[CrossRef](#)]
145. Yu, X.; Wang, S.; Zhang, X.; Qi, A.; Qiao, X.; Liu, Z.; Wu, M. Heterostructured nanorod array with piezophototronic and plasmonic effect for photodynamic bacteria killing and wound healing. *Nano Energy* **2018**, *46*, 29–38. [[CrossRef](#)]
146. Karlsson, J.; Atefyekta, S.; Andersson, M. Controlling drug delivery kinetics from mesoporous titania thin films by pore size and surface energy. *Int. J. Nanomed.* **2015**, *10*, 4425–4436. [[CrossRef](#)] [[PubMed](#)]
147. Gupta, B.; Poudel, B.K.; Ruttala, H.B.; Regmi, S.; Pathak, S.; Gautam, M.; Jin, S.G.; Jeong, J.H.; Choi, H.G.; Ku, S.K.; et al. Hyaluronic acid-capped compact silica-supported mesoporous titania nanoparticles for ligand-directed delivery of doxorubicin. *Acta Biomater.* **2018**, *80*, 364–377. [[CrossRef](#)]
148. Guo, Z.; Zheng, K.; Tan, Z.; Liu, Y.; Zhao, Z.; Zhu, G.; Ma, K.; Cui, C.; Wang, L.; Kang, T. Overcoming drug resistance with functional mesoporous titanium dioxide nanoparticles combining targeting, drug delivery and photodynamic therapy. *J. Mater. Chem. B* **2018**, *6*, 7750–7759. [[CrossRef](#)]
149. Nakayama, M.; Sasaki, R.; Ogino, C.; Tanaka, T.; Morita, K.; Umetsu, M.; Ohara, S.; Tan, Z.; Nishimura, Y.; Akasaka, H.; et al. Titanium peroxide nanoparticles enhanced cytotoxic effects of X-ray irradiation against pancreatic cancer model through reactive oxygen species generation in vitro and in vivo. *Radiat. Oncol.* **2016**, *11*, 91. [[CrossRef](#)]
150. Dai, Z.; Song, X.Z.; Cao, J.; He, Y.; Wen, W.; Xu, X.; Tan, Z. Dual-stimuli-responsive TiO_x/DOX nanodrug system for lung cancer synergistic therapy. *RSC Adv.* **2018**, *8*, 21975. [[CrossRef](#)]



© 2019 by the authors. Licensee MDPI, Basel, Switzerland. This article is an open access article distributed under the terms and conditions of the Creative Commons Attribution (CC BY) license (<http://creativecommons.org/licenses/by/4.0/>).